January 2021

Seismic Response Of Liquid-Filled Thin-Walled Steel Cylindrical Tanks

Wiriyachai Roopkumdee

SEISMIC RESPONSE OF LIQUID-FILLED THIN-WALLED STEEL CYLINDRICAL TANKS

by

Wiriyachai Roopkumdee

Bachelor of Engineering, King Mongkut's University of Technology Thonburi, 2010

Master of Art, Western Kentucky University, 2014

Master of Science, University of North Dakota, 2017

A Dissertation

Submitted to the Graduate Faculty

of the

University of North Dakota

in partial fulfillment of the requirements

for the degree of

Doctor of Philosophy

Grand Forks, North Dakota

December

2021

This dissertation, submitted by Wiriyachai Roopkumdee in partial fulfillment of the requirements for the Degree of Doctor of Philosophy in Civil Engineering from the University of North Dakota, has been read by the Faculty Advisory Committee under whom the work has been done and is hereby approved.

_____

Dr. Iraj H.P. Mamaghani (Chairperson)

_____

Dr. Daba Gedafa

_____

Dr. Nabil Suleiman

_____

Dr. I-Hsuan Ho

_____

Dr. Surojit Gupta

This dissertation is being submitted by the appointed advisory committee as having met all of the requirements of the School of Graduate Studies at the University of North Dakota and is hereby approved.

_____

Dr. Chris Nelson, Associate Dean

School of Graduate Studies

_____

Date

PERMISSION

Title Seismic Response of Liquid-Filled Thin-Walled Steel Cylindrical Tanks

Department Civil Engineering

Degree Doctor of Philosophy

In presenting this dissertation in partial fulfillment of the requirements for a graduate degree from the University of North Dakota, I agree that the library of this University shall make it freely available for inspection. I further agree that permission for extensive copying for scholarly purposes may be granted by the professor who supervised my dissertation work or, in his absence, by the Chairperson of the department or the dean of the Graduate School. It is understood that any copying or publication or other use of this dissertation or part thereof for financial gain shall not be allowed without my written permission. It is also understood that due recognition shall be given to me and to the University of North Dakota in any scholarly use which may be made of any material in my dissertation.

Wiriyachai Roopkumdee

December 2021

Table of Contents

LIST OF FIGURES

LIST OF TABLES

ACKNOWLEDGEMENTS

I wish to express my sincere appreciation and gratitude to Dr. Iraj H.P. Mamaghani, my advisor, for his guidance and support throughout my graduate academic career. My sincere thanks also extended to my committee members, Dr. Daba Gedafa, Dr. Nabil Suleiman, Dr. I-Hsuan Ho, and Dr. Surojit Gupta for their valuable support and advice to complete this dissertation.

NOMENCLATURE

FEM	Finite Element Method
PGA	Peak Ground Acceleration
g	Gravitational Acceleration ≈ 9.81 m/s^2
f_i	ith natural frequency in cycles per unit time
$\boldsymbol{\zeta}$	Damping Ratio
$\boldsymbol{a_0}$	Mass Coefficient
$\boldsymbol{\sigma_{cr}}$	Buckling Stress of Thin-Walled Steel Cylindrical Tank
$\boldsymbol{w_0}$	The amplitude of Initial Geometric Imperfection
CFDST	Concrete-Filled Double-Skin Tube
SSTWT	Single-Skin Thin-Walled Tank
DSTWCT	Double-Skin Thin-Walled Composite Tanks with infill concrete between the inner and outer wall

LIST OF PUBLICATIONS

Peer-Reviewed Journal Papers

1) **Roopkumdee, W.**, Mamaghani H.P. I., (2019). Evaluation of Seismic Design and Buckling Strength of Liquid-Filled Steel Cylindrical Tanks. International Journal of Modern Engineering, 19(1), 53-59.

2) **Roopkumdee, W.**, Mamaghani H.P. I., (2021). Seismic Analysis of Perfect and Imperfect Cylindrical Liquid Storage Tanks. *International Journal of Civil Infrastructure*, 4, 173-179.

3) **Roopkumdee, W.**, Mamaghani H.P. I., (2021). Behavior of Thin-Walled Uniform and Graded Thickness Steel Tubular Columns under Lateral Load Impact, ASCE,. (under review).

4) **Roopkumdee, W.**, and Mamaghani, I. H. P. (2021). Seismic Analysis of Double-Skin Thin-Walled Composite Tank (DSTWCT). *Engineering Structures*, (to be submitted).

Peer-Reviewed Conferences

1) **Roopkumdee, W.**, Mamaghani, I.H.P. (2018) Buckling Strength of Liquid-Filled Steel Cylindrical Tanks under Static and Seismic Loads, 11th National Conference on Earthquake Engineering, June 25-29, 2018, Los Angles, California. Paper No. 59.

2) **Roopkumdee, W.**, and Mamaghani, I.H.P., (2018) Seismic Design and Buckling Strength Evaluation of Liquid-Filled Steel Cylindrical Tanks, ". In 6th IAJC International Conference (**Best Paper Award**), Paper ID: 067, October 11-14, Orlando, Florida, ISBN 978-1-60643-379-9.

3) **Roopkumdee, W.**, and Mamaghani, I.H.P., (2019) Seismic Design and Buckling Strength Evaluation of Liquid-Filled Steel Cylindrical Tanks, Tenth International Structural Engineering and Construction Conference (ISEC-10), May 20-25, 2019.

4) **Roopkumdee, W.**, Mamaghani, I.H.P. (2021). Seismic Resistance and Buckling Strength of Steel Cylindrical Tanks, *Structural Stability Research Council (SSRC) virtual conference*, April 12-16, 2021.

5) **Roopkumdee, W.**, Mamaghani, I.H.P. (2021). Seismic Resistance and Buckling Strength of Cylindrical Steel Liquid Storage Tanks, The *6th International Conference on Civil Structural and Transportation Engineering (ICCSTE'21*) *virtual conference*, May 17-19, 2021, Paper ID 134.

6) Mamaghani, I.H.P., **Roopkumdee, W.** (2021). Seismic Response of LNG Storage Tanks under Earthquake Excitations, The *6th International Conference on Civil Structural and Transportation Engineering (ICCSTE'21*), Niagara Falls, Canada – May 17-19, 2021, Paper ID 141.

ABSTRACT

Seismic response plays an important role in the design of liquid-filled thin-walled steel cylindrical tanks because of the small thicknesses of the walls as compared to their diameter. The liquid-filled thin-walled cylindrical tanks are vulnerable when they are subjected to earthquake accelerations. This dissertation aims to estimate and improve the seismic buckling strength of the liquid-filled thin-walled steel cylindrical tanks under earthquake excitation. The structural response to the base excitation is modeled using the concept of effective earthquake forces. The time steps in numerical analysis are divided to be small enough to accurately capture the periods of oscillations. The finite element method (FEM) is compared with experimental results and theoretical equations available in the literature to ensure the accuracy of the numerical analysis. Based on the extensive parametric study, seismic design equations and design curves representing the interaction effects of the diameter-to-thickness (*D/t)* and height-to-diameter *(H/D)* ratios for the liquid-filled thin-walled steel cylindrical tanks of various geometries subjected to different earthquakes are presented and discussed. Results reveal that the *D/t* ratio is an important parametric factor of the seismic buckling strength of the liquid-filled thin-walled cylindrical tank. The dynamic buckling capacity of the tank decreases significantly when the *D/t* ratio increases. An increase in the *H/D* ratio also seems to have a negative effect on the seismic buckling strength; however, its effect is less significant compared to the *D/t* ratio. The effects of geometrical imperfection on the seismic buckling strength of liquid-

filled thin-walled cylindrical tanks. This study discovers that the seismic buckling strength of the tanks decreases significantly as the amplitudes of initial geometric imperfection are included. This study also introduces the improvement of seismic buckling strength of liquid-filled thin-walled cylindrical tanks due to vertical stiffeners. It is concluded that the vertical stiffeners improve the seismic buckling strength of the liquid-filled thin-walled steel cylindrical tanks when they are subjected to horizontal earthquake excitation. This study concludes that vertical stiffeners can improve the seismic buckling strength by at least 10% of the critical peak ground acceleration (PGA) of unstiffened liquid-filled thin-walled steel cylindrical tanks. Finally, this study proposes the new design criterion of the liquid-filled thin-walled steel cylindrical tanks which is the double-skin thin-walled composite tanks (DSTWCTs). The DSTWCT is constructed to have the same diameter (D) and height (H) as a single-skin thin-walled tank (SSTWT) with an equal volume of steel. DSTWCT consists of two skins which are inner and outer walls. The inner wall diameter of DSTWCT is equal to the diameter of SSTWT. The seismic design and numerical finite element models of DSTWCT are proposed. It is concluded that the seismic buckling capacity of DSTWCT substantially improves when the gap between double skins of DSTWCT is filled with concrete up to 50% of the height of the tank. The location of the seismic buckling of DSTWCT occurs at the hollow sections just above the surface of infill concrete and moves to the higher location as the concrete-filled ratio increases which in turn results in improved seismic buckling strength and ductility.

CHAPTER 1 Introduction

1.1 Liquid-Filled Thin-Walled Steel Cylindrical Tanks

Seismic response plays an important role in the design of liquid-filled thin-walled steel cylindrical tanks because of the small thicknesses of the walls as compared to their diameter. The liquid-filled thin-walled steel cylindrical tanks are vulnerable when they are subjected to horizontal earthquake accelerations. The damages of petroleum storage tanks were reported due to the Long Beach earthquake of 1933, the Kern County earthquake of 1952, the Alaska earthquake of 1964, the San Fernando earthquake of 1971, the Imperial Valley earthquake of 1979, the Coalinga earthquake of 1983, the Loma Prieta earthquake of 1989, the Landers earthquake of 1992, the Northridge earthquake of 1994, and the Kobe earthquake of 1995 (Cooper and Wachholz, 1999). From published reports, the seismic buckling of cylindrical steel tank walls was observed after the Emilia earthquake of 2012 (Buratti and Tavano, 2014) and the South Napa earthquake of 2014 (Fisher et al., 2016). The American Lifelines Alliance (2001) reported the failure modes of steel storage tanks subjected to past earthquakes, which are roof damage, foundation failure, manhole failure, hydrodynamic pressure failure, piping failure anchorage failure, and shell buckling. This study investigated the shell buckling mode of the liquid-filled thin-walled steel cylindrical tanks subjected to horizontal earthquake accelerations. Liquid storage tanks are subjected to horizontal and vertical ground accelerations during earthquakes. These earthquake ground accelerations may cause damages to the liquid storage tanks. Spillage of toxic liquid from the liquid storage tanks could cause a serious threat to human health and the environment. Additionally, the failure of tanks that contain an inflammable substance such as petroleum has frequently led to uncontrolled fires which occurred due to Niigata and Alaska earthquakes in 1964 (Priestley et al., 1986).

The hydrodynamic behavior of liquid-filled thin-walled steel cylindrical tanks when the cylindrical tanks are subjected to earthquakes can be distinguished into two types (Housner, 1963). First, in the impulsive mode, a mass of water is rigidly attached to the tank at the proper height. Second, in the convective mode, the horizontal accelerations from the tank excite a mass of water into oscillations. To investigate the hydrodynamic response of liquid-filled thin-walled tanks under horizontal excitation, the impulsive and convective modes should be investigated separately (Housner, 1963). However, seismic buckling modes usually arise due to the impulsive mode rather than the convective mode (Malhotra and Velestsos, 1994). Morita et al. (2003) and Natsiavas and Babcock (1987) proved that this buckling mode arises mostly from the impulsive action of the hydrodynamic response of the liquid; the sloshing action may contribute to the occurrence of this type of buckling, but it is not the main cause. The buckling behavior of steel tanks subjected to seismic excitation from experiments and computations can be classified as elasto-plastic buckling and elastic buckling. The elasto-plastic buckling behavior is associated with elephant foot buckling, which is characterized by an outward bulge just above the base of the tank (Handam, 2005). Diamond shape buckling at the bottom of the tank has also been described as elastic buckling (Handam, 2005). Elastic buckling includes buckling at the top part of the cylindrical tank and shear buckling of the shell. Shear buckling for tanks in the elastic range has been reported by Teng and Rotter (2004). The elephant foot and diamond shape buckling are represented in Figs. 1(a) and 1(b), respectively.

(a) (b)

Fig. 1.1. Buckling shapes: (a) Elephant foot buckling, (b) diamond shape buckling (courtesy of University of California at Berkeley).

Previous research was conducted to investigate the seismic local buckling of unstiffened steel cylindrical tanks using experimental study and finite element method (FEM). The buckling of tall steel cylindrical wine storage tanks was investigated using a shaking table to generate the characteristics of the 1980 Livermore earthquake (Niwa and Clough,1982). Housner and Haroun (1979) conducted the force vibration tests to study the dynamic response of full-scale liquid-filled steel cylindrical tanks. Seismic buckling strengths of different sizes of cylindrical steel tanks under earthquake loads were studied using FEM (Virella et al., 2006; Diermane, 2014; Roopkumdee and Maamghani, 2018, 2019, 2021). Virella et al. (2006) used a commercial finite element program ABAQUS to study dynamic buckling of the anchored steel tanks with the height-to-diameter ratio (*H/D*) less than 1.0, finding that the seismic buckling occurred at peak ground acceleration (PGA) between 0.25g to 0.35g. Djermane et al. (2014) evaluated the PGA values that caused the instability state of the steel cylindrical tanks using FEM. Sobhan et al. (2017) used nonlinear static pushover to investigate the buckling behavior of the anchored steel tanks, finding that bi-

directional excitation obtained from static pushover analysis is similar to that obtained from dynamic buckling analysis. Sezen et al. (2008) used the ANSYS computer program to study liquefied gas-structure interaction and a simplified model of three tanks in Turkey that experienced an earthquake on August 17, 1999; they reported that shear and bending moments are overestimated if the fluid is modeled as a single rigid mass.

1.2 Problem Statement

Researchers investigated the behavior of the liquid-filled thin-walled steel cylindrical tanks under seismic loading. All these studies addressed the response of single-layer geometrical perfect unstiffened steel cylindrical tanks (Malhotra and Veletsos, 1994; Natsiavas and Babcock, 1987; Niwa and Clough, 1982; Virella et al., 2006; Diermane et al., 2014; Sobhan et al., 2017; Sezen et al., 2008; Virella et al., 2005; Roopkumdee, 2017; Johnson, 2019). To overcome this deficiency and ensure the seismic response of the liquid-filled thin-walled steel cylindrical tanks, this dissertation investigates and proposes the intensive parametric studies of the liquid-filled thin-walled steel cylindrical tanks under earthquake excitations.

The main concern in seismic resistance of the liquid-filled thin-walled steel cylindrical tank is the interaction effects between various diameter-to-thickness (D/t) and height-to-diameter (H/D) ratios when the liquid-filled thin-walled steel cylindrical tanks are subjected to different characteristics of the earthquake excitations. This study expanded the range of parametric studies of D/t and H/D ratios. The three different recorded earthquake accelerations were applied to the liquid-filled thin-walled steel cylindrical tank to propose the new design equation and general behaviors of the liquid-filled thin-walled steel cylindrical tanks. The other concern of the seismic resistance design of the liquid-filled thin-walled steel cylindrical tank is the geometrical imperfection. The seismic buckling strength of the potential construction with the initial

geometrical imperfection was investigated, and the new seismic design equation for the liquid-filled thin-walled steel cylindrical tank with the initial geometrical imperfection was proposed. The other concern is the seismic strength improvement of the liquid-filled thin-walled steel cylindrical tank due to the vertical stiffeners. the new design equation and general behaviors of the stiffened liquid-filled thin-walled steel cylindrical tanks are proposed in this study. The new seismic design criterion for the liquid-filled thin-walled steel cylindrical tanks was proposed in terms of the double-skin thin-walled composite tanks (DSTWCTs). The DSTWCT was constructed to have the same diameter (D) and height (H) as a single-skin thin-walled tank (SSTWT) with an equal volume of steel. The seismic buckling capacity of DSTWCT substantially improves when the gap between double skins of DSTWCT is filled with concrete up to 50% of the height of the tank.

1.3 Objectives

This study aims to propose the seismic design equations and investigate the seismic response of the liquid-filled thin-walled steel cylindrical tanks under different influences. This study has four main objectives: (1) investigating seismic behavior of liquid-filled thin-walled steel cylindrical tanks under different diameter-to-thickness (D/t) and height-to-diameter (H/D) ratios, (2) seismic analysis of geometrical imperfect liquid-filled thin-walled cylindrical tanks, (3) seismic buckling evaluation of unstiffened and stiffened liquid-filled thin-walled steel cylindrical tanks, and (4) design and analysis of the seismic response of double-skin thin-walled composite tanks (DSTWCTs).

1.4 Organization of the Dissertation

This dissertation consists of six chapters, as shown in Fig. 1.2. The present chapter presents the general introduction about the existent knowledge of the seismic behavior of liquid-filled thin-walled steel cylindrical tanks and the need for proposed new parametric studies.

Chapter 2 deals with the seismic behavior of liquid-filled thin-walled steel cylindrical tanks under different diameter-to-thickness (*D/t*) and height-to-diameter (*H/D*) ratios when they are subjected to the different characteristics of the earthquake excitation. In chapter 3, the seismic buckling capacities of the initial geometrical imperfect liquid-filled thin-walled steel cylindrical tanks are investigated to compare with the geometrical perfect liquid-filled thin-walled steel cylindrical tanks. In chapter 4, the seismic buckling behavior of the stiffened liquid-filled thin-walled steel cylindrical tanks is investigated. In chapter 5, the new methodology of the seismic resistance of liquid-filled thin-walled steel cylindrical tanks is proposed, which is the double-skin thin-walled composite tanks (DSTWCTs). Finally, the conclusions and future work are summarized in Chapter 6.

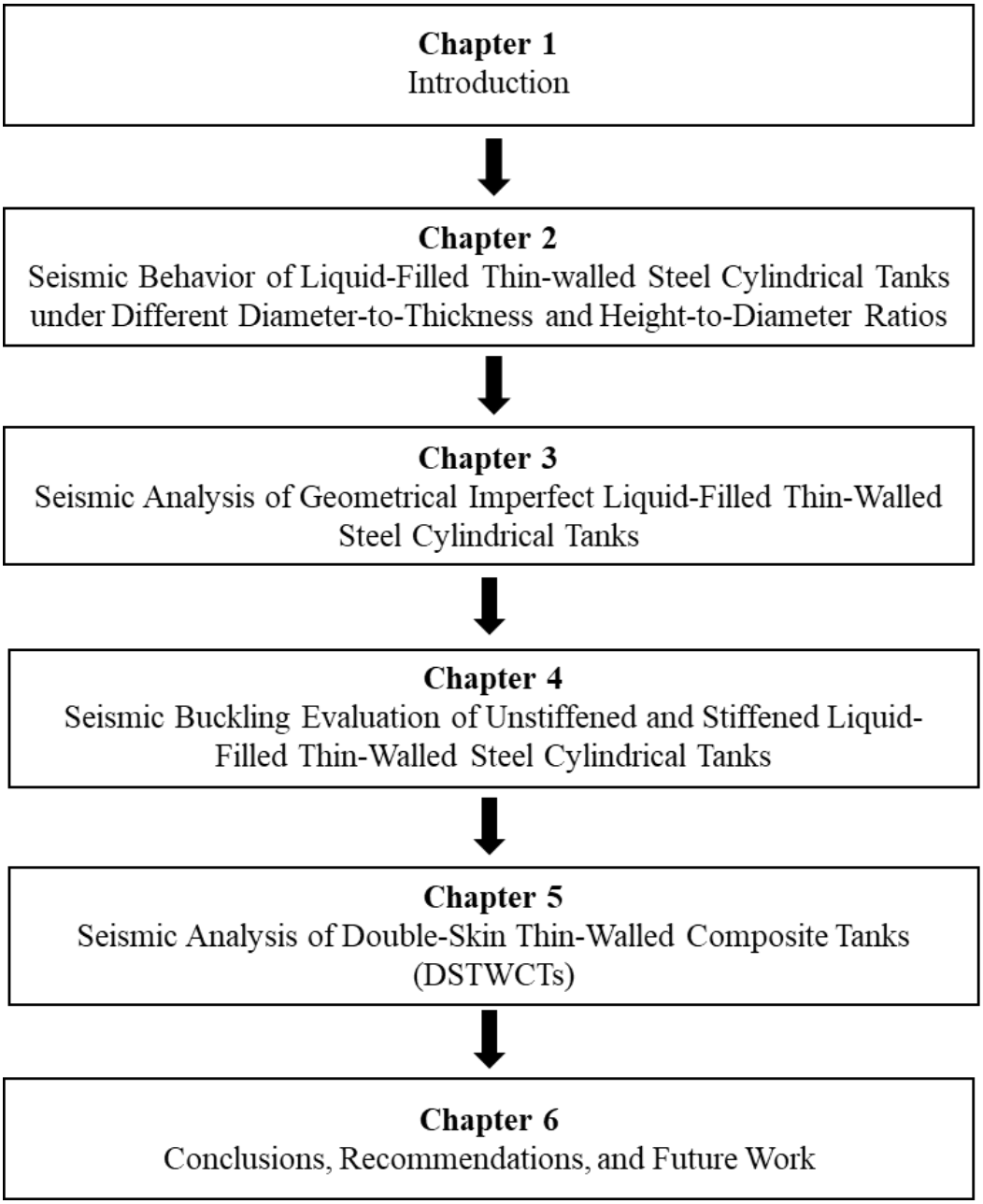

Fig. 1.2. Organization of the Chapters.

CHAPTER 2 Seismic Behavior of Liquid-Filled Thin-Walled Steel Cylindrical Tanks under Different Diameter-to-Thickness and Height-to-Diameter Ratios

2.1 Introduction

This chapter aims to develop a practical seismic design equation to estimate the buckling strength of the liquid-filled thin-walled cylindrical tanks subjected to earthquake loads. Pseudo-Equilibrium path criterion is used to evaluate buckling strength. Finite element analysis is performed using ANSYS computer program. The modeling method, appropriate element types, and the necessary number of elements to use in numerical analysis are recommended. The structural response to the base excitation is modeled using the concept of effective earthquake forces; therefore, acceleration input was to create an acceleration field acting on all the nodes of the model. In addition, the time steps are divided to be small enough to accurately capture the periods of oscillations. Characteristics of earthquake excitations play an important role in the buckling strength of liquid-filled thin-walled steel cylindrical tanks. Based on the extensive parametric study, seismic design equations and design curves representing the interactions of *D/t* and *H/D* ratios for the cylindrical tanks of various geometries subjected to El Centro 1940, Parkfield 2004, and Northridge 1994 earthquakes are presented and discussed. Results revealed that the *D/t* ratio is an important parametric factor of the seismic buckling strength of the liquid-filled thin-walled cylindrical tank. The dynamic buckling capacity of the tank decreases significantly when the *D/t* ratio increases. An increase in the *H/D* ratio also decreases the seismic buckling strength; however, its effect is less significant compared to the *D/t* ratio.

2.2 Methodology

2.2.1 Numerical Model

Five different geometric configurations of the cylindrical tanks are analyzed with height-to-diameter (*H/D*) ratios of 0.43, 0.67, 1.00, 1.46, and 2.41 and the diameter-to-thickness (*D/t*) ratios of 910, 1013, 1216, 1612, and 2130 to investigate the buckling behaviors of various sizes of the cylindrical tanks. The geometries of the cylindrical tanks are illustrated in Table 2.1. and Fig. 2.1. FEM meshing of model A is illustrated in Figure 2.2.

Table 2.1. Geometries of the liquid-filled thin-walled steel cylindrical tanks.

Model	*H* (m)	*D* (m)	*t* (mm)	H_r (m)	*H/D*	*D/t*
A	6.1	9.1	10.0	0.853	0.67	910
B	18.3	7.6	7.5	0.713	2.41	1013
C	15.2	15.2	12.5	1.425	1.00	1216
D	20.0	13.7	8.5	1.284	1.46	1612
E	9.1	21.3	10.0	2.000	0.43	2130

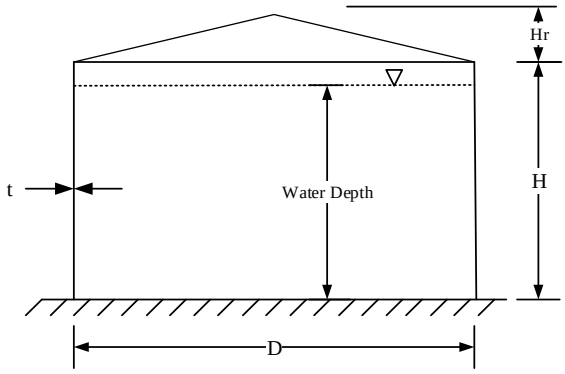

Fig. 2.1. Cylindrical tank geometry.

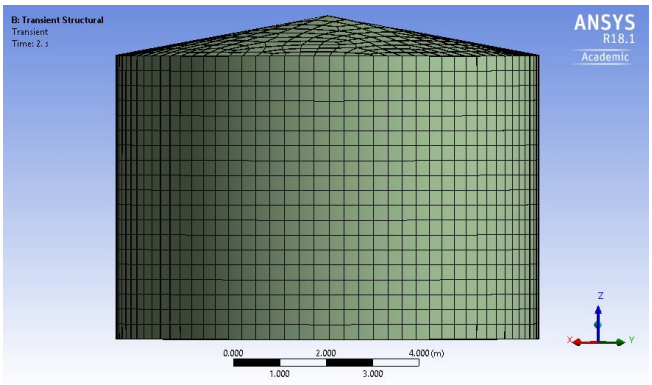

Fig. 2.2. FEM meshing of model A.

The material for all cylindrical storage tanks is steel with a modulus of elasticity, E = 200 GPa, Poisson's ratio, ν = 0.3, and the mass density, ρ = 7,850 kg/m^3. Bilinear isotropic hardening of the steel is included with the yield stress of 345 MPa and the tangent modulus of 13.79 GPa, which is equal to ASTM A572 steel (ASTM, 2018). The liquid-filled inside the cylindrical tanks is water with the bulk modulus of 2,068.4 MPa, and the mass density of 1,000 kg/m^3. The water depth of each model is 90% of the height of the tank.

All cylindrical tanks are considered to be fixed at the base and free on the top. The histogram of earthquake excitation in terms of acceleration is applied to every node of cylindrical tanks. Therefore, the structural response to the base excitation was modeled using the concept of effective earthquake forces (Chopra, 2011) as illustrated in Fig. 2.3.

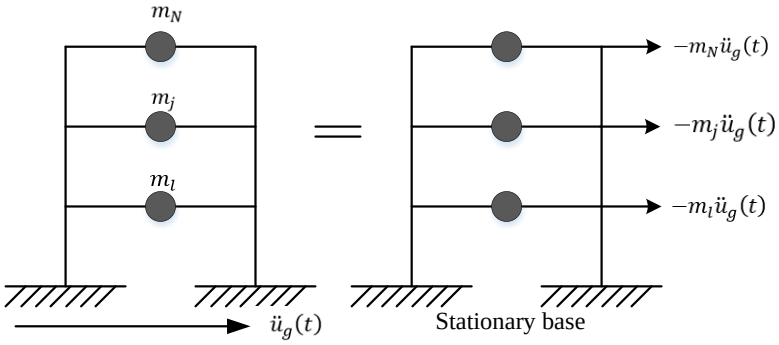

Fig. 2.3. Ground excitation and effective earthquake force (Chopra, 2011).

ANSYS computer program is used to carry all computations. SHELL181 element is used to be the element for the steel cylindrical tanks. SOLID185 element is used to be the element for water-filled inside the cylindrical tanks. SHELL181 is a four-node element with six degrees of freedom at each node (translation in x, y, and z directions, and rotation about x, y, and z axes). SOLID185 is used for 3-D modeling of solid structures. It is defined by eight nodes having three degrees of freedom at each node: translations in the nodal x, y, and z directions (ANSYS, 2009). The elements of SHELL181 for models A, B, C, D, and E are modeled with 4174, 5513, 8838, 7941, and 7198 elements, respectively. The elements of SOLID185 for models A, B, C, D, and E are modeled with 1274, 1542, 2076, 1756, and 1834 elements, respectively.

2.2.2 Verification of Finite Element Method (FEM)

The FEM is compared with experimental results available in the literature (Tazuke, 2002). The tested tank FEM model for the static loading test is shown in Fig. 2.4. The test on static loading is performed on the aluminum tank, measuring 2.5 m in height and 2 m in diameter. The aluminum tank has a wall and bottom of a 2 mm thin plate. Similar to the actual tank, FEM is restrained from the tank uplifting through anchor straps tying the lower part of the sidewall to the shaking table floor (16 pieces of 9-mm-dia stainless steel rods).

The effective mass and the structure period of vibration are conducted as a lumped mass model. The wall of the storage tank is conducted using element SHELL 181. The liquid-filled inside the tanks is conducted using SOLID 185. The element has plasticity, hyper elasticity, stress stiffening, creep, large deflection, and large strain capabilities. It has also mixed formulation capability for simulating deformations of nearly incompressible elastoplastic materials, and fully incompressible hyperplastic materials. The 16 pieces of 9 mm diameter

stainless steel are conducted using LINK 180. LINK180 is a 3-D spar that is useful in a variety of engineering applications. The element can be used to model trusses, sagging cables, links, springs, and so on. The element is a uniaxial tension-compression element with three degrees of freedom at each node: translations in the nodal x, y, and z directions (ANSYS, 2009). For the static verification, the FEM consists of 3,883 SHELL 181 elements, 4,756 SOLID 185 elements, and 320 LINK 180 elements. Similar to the available experiment, the material properties of the LNG tank wall are designed as aluminum (6061-T6). The material properties of the tank wall and liquid-filled inside the tank are listed in Table 1.

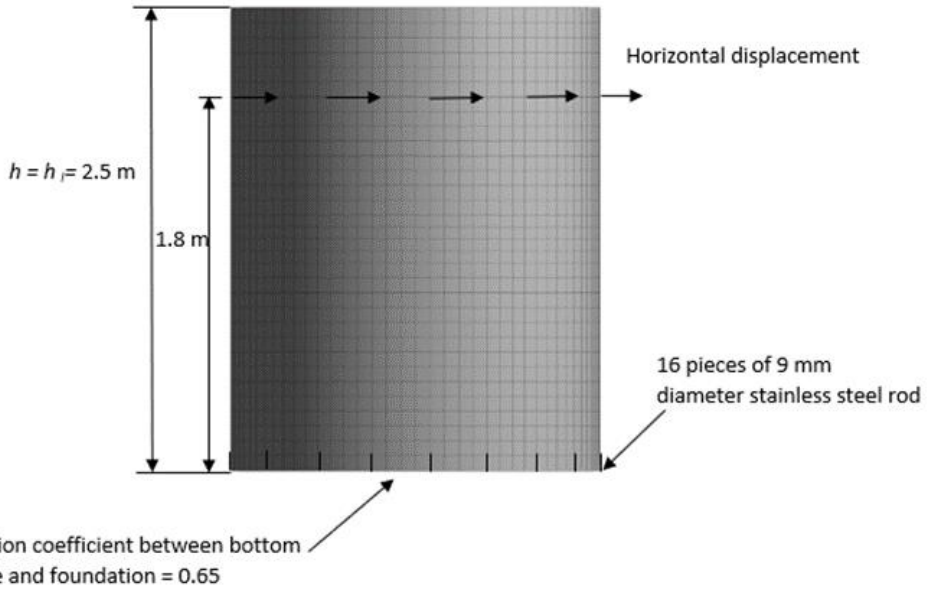

Fig. 2.4. FEM meshing of a tested tank (Tazuke, 2002).

Table 2.2. Material properties of the verified model.

Material properties	Value
Young's modulus (6061-T6)	68.9 GPa
Yield stress (6061-T6)	276 MPa
Hardening modulus (6061-T6)	2.04 GPa
Shear modulus (6061-T6)	26 GPa
Poisson's (6061-T6)	0.33
Density (6061-T6)	2,700 kg/m^3
Friction coefficient between base and foundation	0.65
Density (liquid-filled)	1,000 kg/m^3
Internal pressure	5,390 Pa

Fig. 2.5. illustrates the post-buckling deformation of the overall structure. Fig. 2.6. shows that the elephant foot buckling using FEA is located at the same location as the experimental result. The maximum von-Mises stress at the EFB location is 296 MPa, which exceeds the yield stress of the material (6061-T6). Fig. 2.7. compares horizontal load versus horizontal displacement at a reference location (1,800 height). The results for FEA show a good agreement with the experimental results as shown in Fig. 2.7.

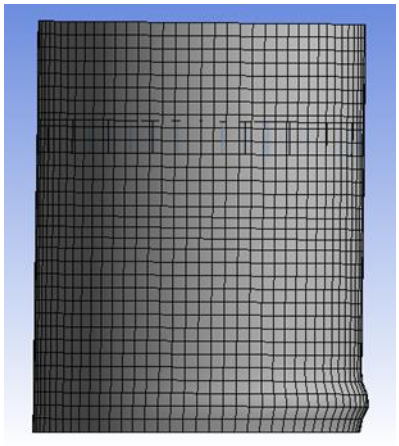

Fig. 2.5. Overall deformed shape of the LNG tank

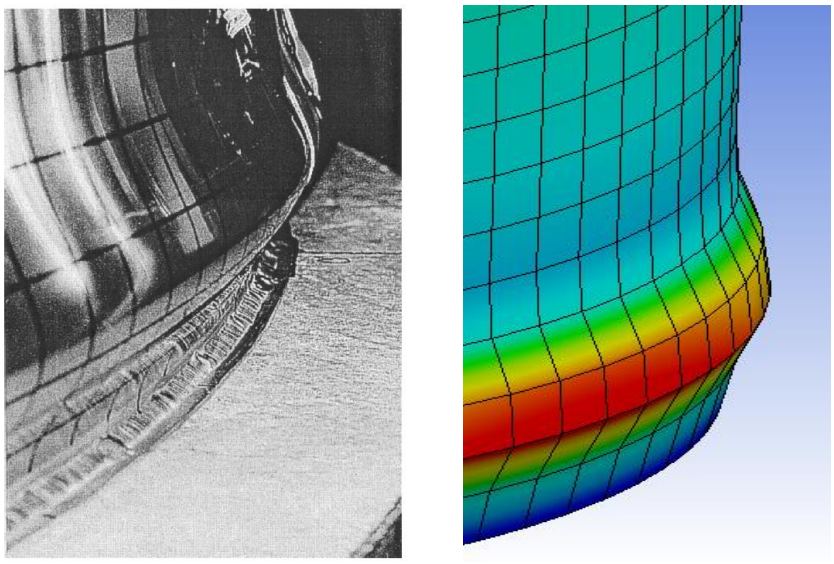

(a) (b)

Fig. 2.6. Overall deformed shape of the tank: (a) experiment (Tazuke, 2002), (b) FEM

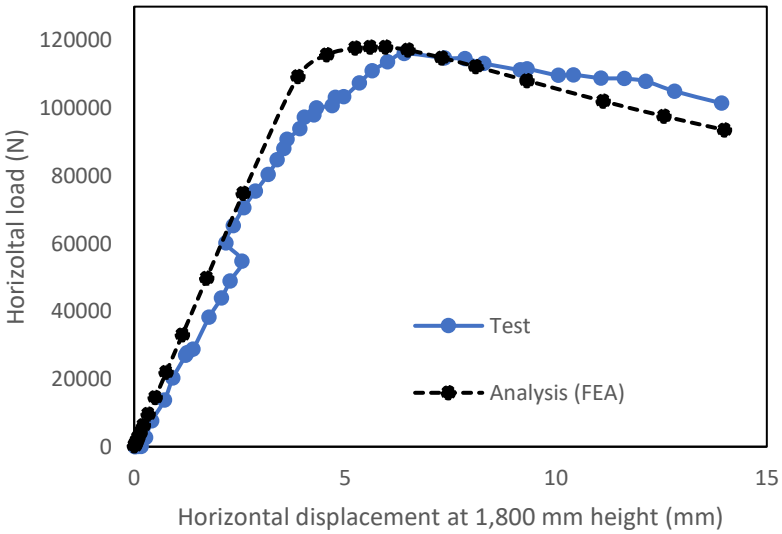

Fig. 2.7. Comparison between FEA with test results (Tazuke, 2022) in monotonic static loading test.

2.2.2 First Natural frequencies and Damping Ratios

2.2.2.1 Modal Analysis

Modal analysis is the method to investigate the vibration characteristics in terms of natural frequencies and mode shapes of the cylindrical tanks in the ANSYS computer program. The natural frequencies and mode shapes are the parameters that are used to find mass and stiffness coefficients for the Rayleigh damping method in the transient analysis. In the modal analysis, a structure is assumed to be a free vibration system, so the external force and damping do not exist in the model analysis. The equation of motion for an undamped system vibrating freely is expressed in matrix notation as in Eq. (2.1).

$$[M]\{\ddot{u}\} + [K]\{u\} = \{0\} \tag{2.1}$$

where [M] is structural mass matrix, [K] is structural stiffness matrix, {ü} is nodal acceleration vector, and {u} is a nodal displacement vector.

For a linear system, free vibration will be harmonic of the form in Eq. (2.2).

$$\{u\} = \{\phi_i\} \cos \omega_i t \tag{2.2}$$

The Eq. (2.1) becomes Eq. (2.3):

$$(-\omega^2[M] + [K])\{\phi_i\} = \{0\} \tag{2.3}$$

Eq. (2.3) is satisfied if the quantity of $(-\omega^2[M] + [K])$ or $\{\phi_i\}$ is equal to zero. However, the condition that the eigenvector is zero, $\{\phi_i\} = 0$, is trivial; therefore, this condition is not of interest. The condition of interest is Eq. (2.4).

$$|[K] - \omega^2[M]| = 0 \tag{2.4}$$

The finite element simulation may solve up to n values of ω^2 and $\{\phi_i\}$ to satisfy Eq. (2.3) where n is the number of degrees of freedoms (DOFs). In the modal analysis, in ANSYS, the

output is the natural frequencies (f) instead of the natural circular frequencies (ω) which are represented as in Eq. (2.5).

$$f_i = \frac{\omega}{2\pi} \tag{2.5}$$

where f_i is i^{th} natural frequency in terms of cycles per unit time.

2.2.2.2 Damping Ratio

A procedure of Rayleigh Damping was adopted in this study. For simplicity and numerical efficiency, the damping was assumed as Rayleigh mass proportional damping as shown in Eq. (2.6) and Eq. (2.7).

$$[C] = a_0[M] \tag{2.6}$$

$$a_0 = 2\omega_n\zeta_n \tag{2.7}$$

where a_0 is a mass coefficient, and ζ_n is critical damping ratio.

For the steel structure, the critical damping ratio is generally between 2% and 3% (Djermane, et al., 2014). In this study, the value of 2% was adopted. This mass coefficient (a_0) is to be input into the transient analysis to indicate the damping ratio of the structure. The first natural frequencies mass coefficients of each model are represented in Table 2.3.

Table 2.3. First natural frequencies and mass coefficients of the tanks filled with water up to 90% height

Model	**First Natural Frequency (Hz)**	**Mass Coefficient (a_0)**
A	4.259	1.070
B	1.993	0.501
C	2.293	0.576
D	1.824	0.458
E	2.070	0.520

2.3 Nonlinear Seismic Analysis

The transient analysis was used in this study to investigate the seismic behavior of a structure when it is subjected to a time-dependent loading. Inertia and damping effects are considered for the transient dynamic analysis. The equation of motion, Eq. (2.8), is solved by the transient structure simulation in the ANSYS computer program.

$$[M]\{\ddot{u}\} + [C]\{\dot{u}\} + [K]\{u\} = \{F_{(t)}\} \tag{2.8}$$

where $[M]$ is mass matrix, $[C]$ is damping matrix, $[K]$ is stiffness matrix, $\{\ddot{u}\}$ is nodal acceleration vector, $\{\dot{u}\}$ is nodal velocity vector, $\{u\}$ is nodal displacement, $\{F_{(t)}\}$ is load vector, and t is time.

Data sets of earthquake loads of El Centro 1940, Parkfield 2004, and Northridge 1994 are collected from The United States Geological Survey (2017). Numerical values of these earthquakes are in the unit of g, the accelerations due to gravity for the El Centro, Parkfield, and Northridge earthquakes are presented in Fig. 2.8, Fig. 2.9, and Fig. 2.10, respectively.

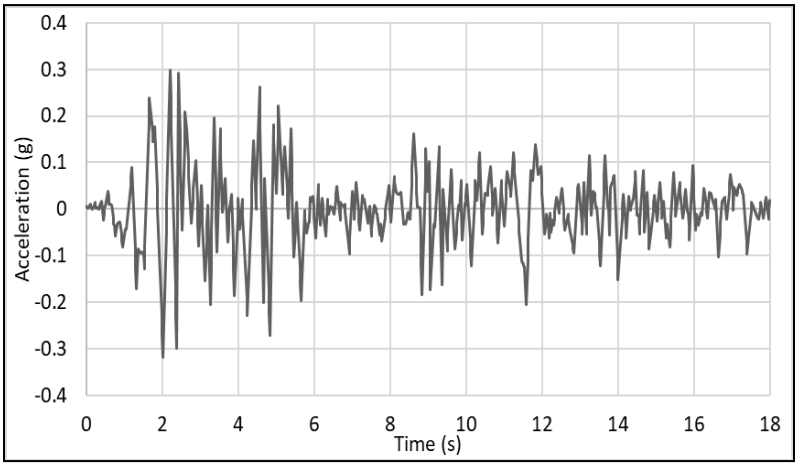

Fig. 2.8. Accelerogram of North-South component of El Centro earthquake, 1940

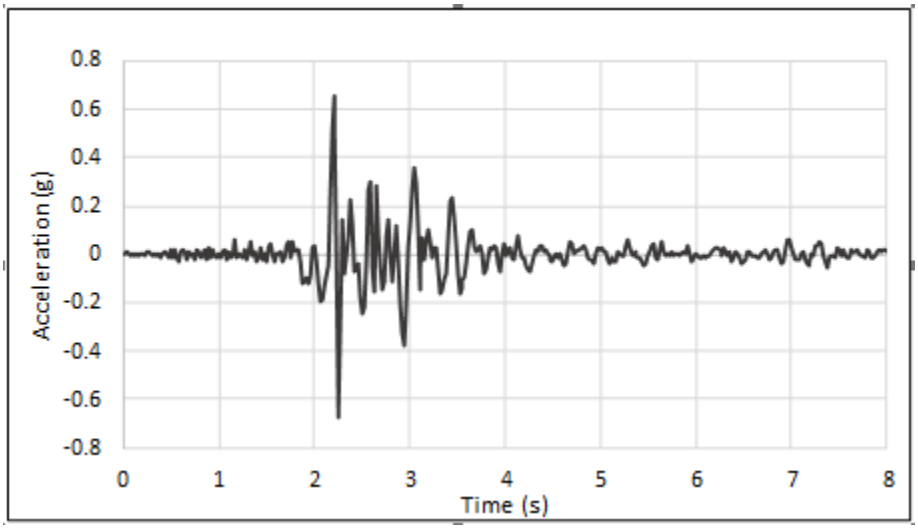

Fig. 2.9. Accelerogram of North-South component of Parkfield earthquake, 2004

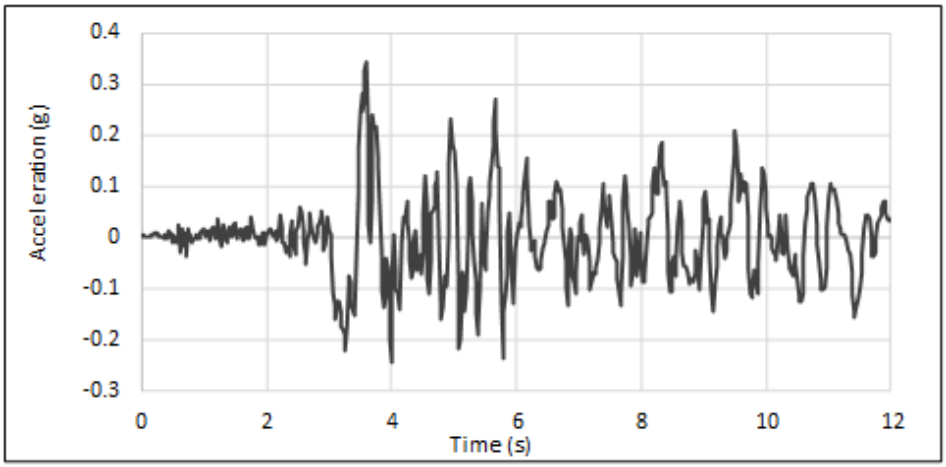

Fig. 2.10. Accelerogram of North-South component of Northridge earthquake, 1994

2.3.1 El-Centro Earthquake

Budiansky and Roth (1962) criterion was used to generate pseudo-equilibrium paths in this study. Buckling instability occurs when a small increase in the pulse intensity causes a strong increase in the rate of deflection. Therefore, different analyses of the structure for several loads (PGAs) must be constructed. The node which gave the maximum displacement of each model was used to find the pseudo-equilibrium path. For example, node 2638 has maximum displacement

when PGA is 0.7g as illustrated in Fig. 2.11. Fig. 2.12(a) illustrates the pseudo-equilibrium paths and the seismic buckling capacities of models A, and C. The seismic buckling capacities of models A and C are 0.72g, and 0.56g, respectively. Fig. 2.12(b) illustrates the pseudo-equilibrium paths and the seismic buckling capacities of model B. The seismic buckling capacity of model B is 0.55g. Fig. 2.12(c) illustrates the pseudo-equilibrium paths and the seismic buckling capacities of models D and E. The seismic buckling capacities of models D and E are 0.15g and 0.075g, respectively.

Transient response curves in terms of nodal displacement with an increase in PGA are also observed in this study. Fig. 2.13 shows the significant jump in the nodal displacement of model C which indicates that the structure is unstable for PGA = 0.6g.

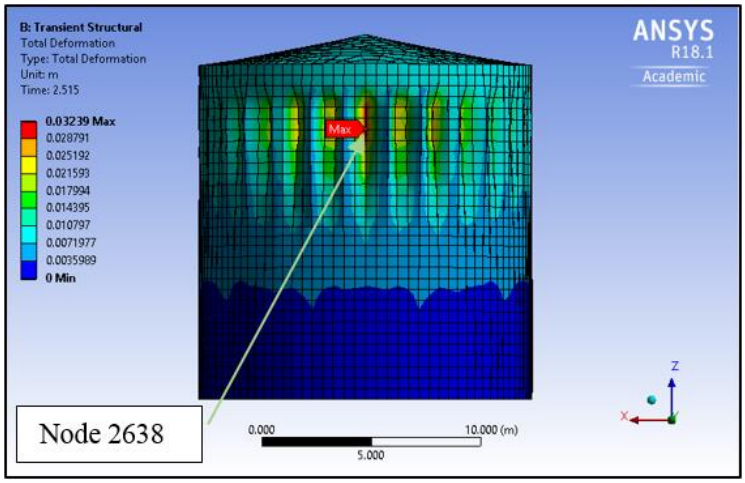

Fig. 2.11. Deformation of model C subjected to El Centro earthquake.

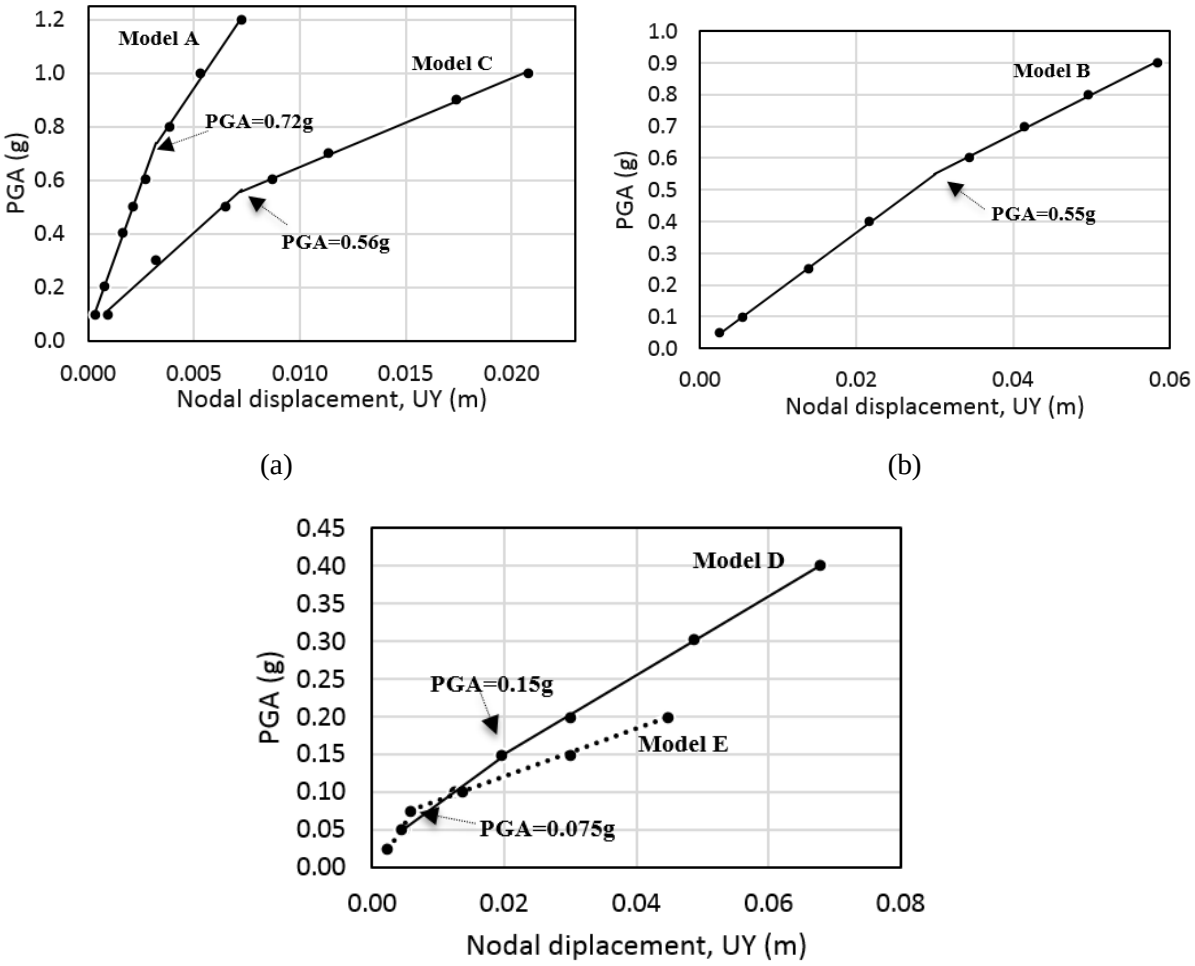

(a) (b)

(c)

Fig. 2.12. Pseudo-equilibrium paths; (a) models A and C, (b) model B, and (c) models D and E.

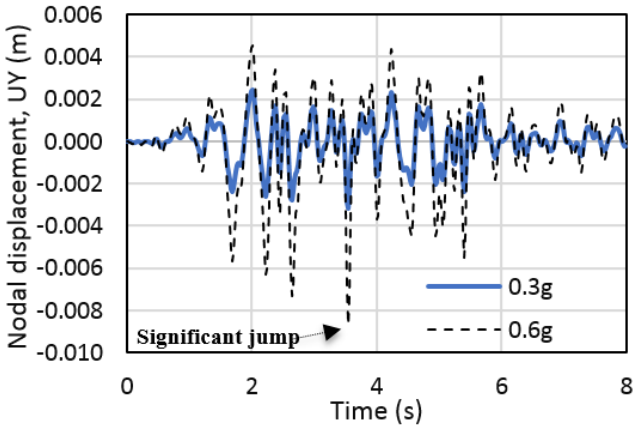

Fig. 2.13. Transient response of model C.

2.3.2 Parkfield Earthquake

Parkfield earthquake was chosen to be one of the applied earthquake excitations to study the seismic buckling strength of liquid-filled thin-walled steel cylindrical tanks due to different characteristics of earthquake excitation. Nodes that gave the maximum displacement to the steel cylindrical tanks when they were subjected to the Parkfield earthquake are nodes 2623, 2876, 5580, 1076, and 1436 for models A, B, C, D, and E, respectively. Fig. 2.14(a) illustrates the pseudo-equilibrium path and the seismic buckling capacity of model A. The seismic buckling capacity of model A is 1.30g. Fig. 12.14(b) illustrates the pseudo-equilibrium paths and the seismic buckling capacities of models C and D. The seismic buckling capacities of models C and D are 0.88g and 0.40g, respectively. Fig. 12.14(c) illustrates the pseudo-equilibrium path and the seismic buckling capacity of model B. The seismic buckling capacity of model B is 1.20g. Fig. 12.14(d) illustrates the pseudo-equilibrium path and the seismic buckling capacity of model E. The seismic buckling capacity of model B is 0.33g.

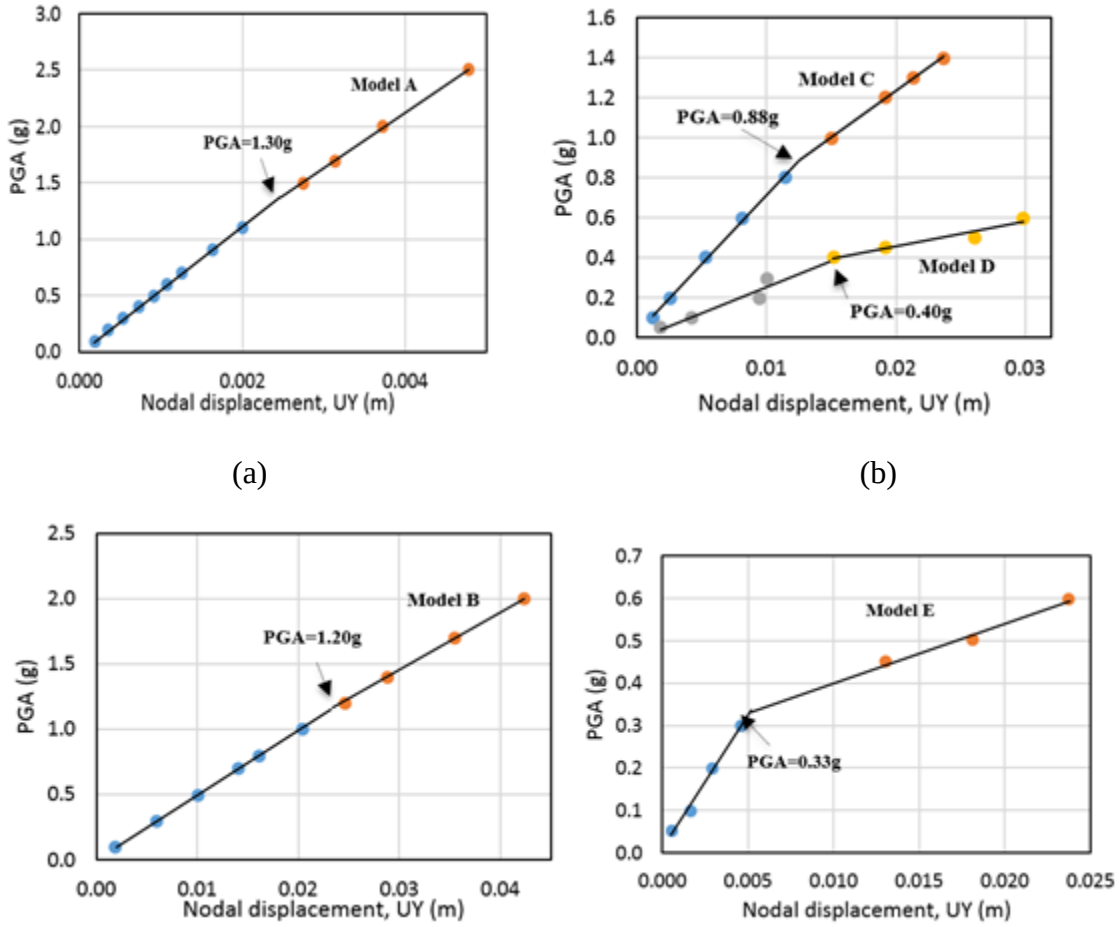

Fig. 2.14. Pseudo-equilibrium paths; (a) model A, (b) models C and D, (c) model B, and (d) model E.

2.3.3 Northridge Earthquake

The results of finite element models using El Centro and Parkfield earthquakes indicate that the seismic buckling capacities decrease when *D/t* ratios increase; however, the effect of the *H/D* ratio could not be simplified. Thus, the Northridge earthquake was included in this study to interpret the uncertain effect of the H/D ratio. Fig. 2.15(a) illustrates the pseudo-equilibrium paths and the seismic buckling capacities of models A and C. The seismic buckling capacities of models A and C are 1.34g and 0.70g, respectively. Fig. 2.15(b) illustrates the pseudo-equilibrium path and

the seismic buckling capacity of model B. The seismic buckling capacity of model B is 0.63g. Fig. 2.15(c) illustrates the pseudo-equilibrium paths and the seismic buckling capacities of models D and E. The seismic buckling capacities of models D and E are 0.21g and 0.20g, respectively. Fig. 2.16 illustrates the significant jumps from transient response curves for model D.

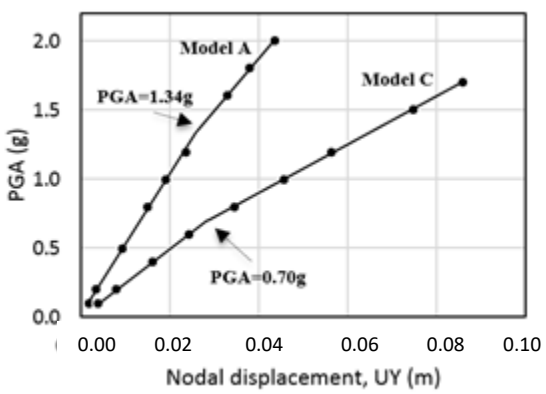

(a)

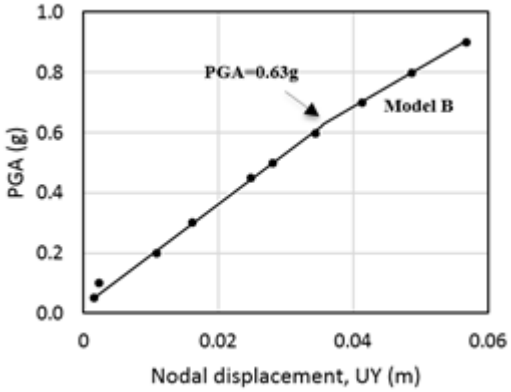

(b)

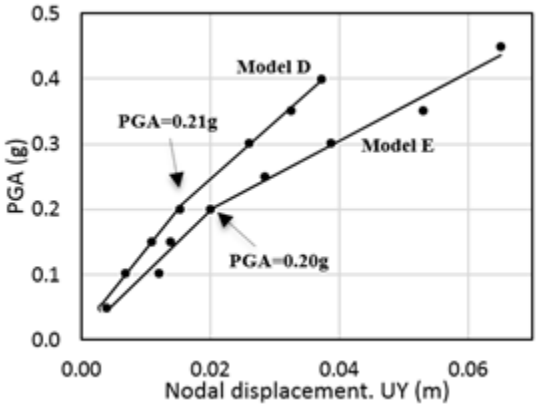

(c)

Fig. 2.15. Pseudo-equilibrium paths; (a) models A and C, (b) model B, and (c) models D and E

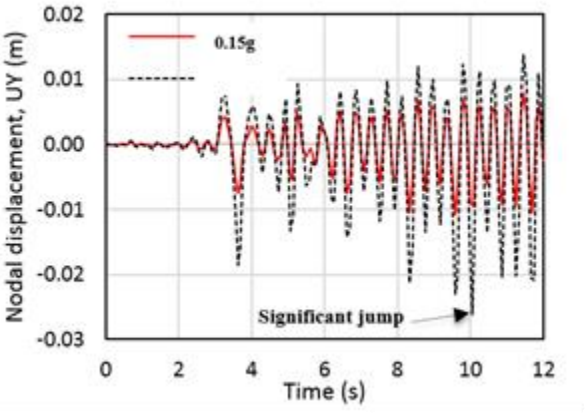

Fig. 2.16. Transient response of model D

2.4 Proposed Design Equation

To estimate the interaction effects of *H/D* and *D/t* ratios on the seismic buckling strengths of the steel cylindrical tanks, a nonlinear regression analysis was used to develop a design equation. From El Centro, Parkfield, and Northridge earthquake cases, the Design equation can be estimated as Eq. (2.9).

$$PGA = -0.2838\ln(H/D) - 2.93(10^{-7})(D/t)^2 + 1.2302 \quad (2.9)$$

R^2 value of Eq. (2.9) is 0.7018. The coefficients of *D/t* and *H/D* ratios are statistically significant at a 95% confident interval.

From Eq. (2.9), the *D/t* ratio has a significant negative effect on the seismic buckling capacity. If the *D/t* ratio increases, the seismic buckling capacity significantly decreases. An increase in the *H/D* ratio also shows a negative effect on seismic buckling capacity; however, when the *H/D* ratio increases the buckling capacities will decrease with a diminishing rate. Eq. (2.9) is estimated from the geometries of the tanks based on this study. Therefore, the estimated design equation may have to be reinvestigated if the dimension of the steel cylindrical tank is not covered by this study.

2.5 Summary

The seismic buckling capacities of liquid-filled thin-walled steel cylindrical tanks were evaluated using various sizes of steel cylindrical tanks. The interaction effects of *D/t* and *H/D* ratios on the dynamic buckling were investigated, and a design equation was proposed. Results show that the *D/t* ratio is an important parametric factor of the seismic buckling strength of the liquid-filled thin-walled steel cylindrical tank. The seismic buckling capacity of the tank decreases significantly when the *D/t* ratio increases. An increase in the *H/D* ratio also seems to have a negative effect on the seismic buckling strength; however, its effect is less significant compared to the *D/t* ratio.

CHAPTER 3 Seismic Analysis of Geometrically Imperfect Liquid-Filled Thin-Walled Steel Cylindrical Tanks

3.1 Introduction

This chapter aims to propose a practical design equation for geometrically imperfect thin-walled steel cylindrical tanks. Both geometrically perfect and imperfect liquid-filled thin-walled steel cylindrical tanks are studied. Numerical analysis was used to evaluate the seismic buckling strength of the thin-walled steel cylindrical tanks. A design equation for estimating the buckling strength of the geometrically perfect thin-walled steel cylindrical tank was developed by using regression analysis on the results listed in chapter 2 as Eq (2.9). The first buckling mode shape obtained by eigenvalue analysis was used as the initially imperfect shape of the cylindrical tanks. To ensure the accuracy of numerical analysis, the buckling stresses of analyzed tanks were verified with the theoretical buckling stresses corresponding to the various diameter-to-thickness, and height-to-diameter ratios. The theoretical static buckling stress for the pin-pin ended cylindrical shells is given by Eq. (3.7). For seismic buckling analysis, Pseudo-Equilibrium path and phase plane criterion were used to evaluate the seismic buckling strength of the liquid-filled thin-walled steel cylindrical tanks. The results show that the seismic buckling strength of the liquid-filled thin-walled steel tanks decreases significantly when the amplitudes of initial geometric imperfection are included. Based on the extensive parametric study, design equations representing the interaction between the D/t, H/D ratios, and initial geometric imperfection for the liquid-filled thin-walled steel cylindrical tanks of various geometries subjected to three different earthquakes are presented and discussed.

3.2 Methodology

3.2.1 Numerical Model

Five different geometric configurations of the thin-walled steel cylindrical tanks were analyzed with height-to-diameter (*H/D*) ratios of 0.43, 0.67, 1.00, 1.46, and 2.41 and the diameter-to-thickness (*D/t*) ratios of 910, 1013, 1216, 1612, and 2130 to investigate the buckling behaviors of various sizes of the thin-walled steel cylindrical tanks. The geometries of the thin-walled steel cylindrical tanks are similar to the geometries of the liquid-filled thin-walled steel cylindrical tanks as illustrated in Table 2.1. The material properties of structural steel and liquid-filled inside the thin-walled steel cylindrical tanks are identical to the material properties as discussed in section 2.2.1.

3.2.2 Verification of Finite Element Method (FEM)

The accuracy of the finite element model using the ANSYS computer program was verified by using the theoretical buckling stress for the pin-pin ended cylindrical shells. If the thin-walled steel cylindrical tank is uniformly compressed in the axial direction as shown in Fig. 3.1, the general solution for very small displacements is given as shown in Eqs. (3.1) to (3.7) (Timoshenko and Gere, 1983; Timoshenko and Woinowsky-Krieger, 1959).

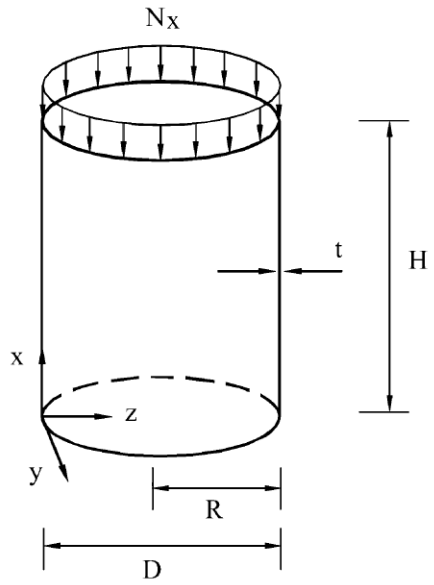

Fig. 3.1. Thin-walled steel cylindrical tank subjected to axial load (Kim and Kim, 2002).

$$u = A \sin n\theta \cos \frac{m\pi x}{H} \tag{3.1}$$

$$v = B \sin n\theta \cos \frac{m\pi}{H} \tag{3.2}$$

$$w = C \sin n\theta \cos \frac{m\pi}{H} \tag{3.3}$$

where *A*, *B*, and *C* are constants. H is the height of the thin-walled steel cylindrical tank. n and m are the buckling number of circumferential and longitudinal half-waves, respectively. When the pin-pin supported conditions of w = 0 and $d^2w/dx^2 = 0$ are used at the ends, the critical stress is obtained as

$$\sigma_{cr} = \frac{N_x}{t} = \frac{RE}{S(1-v^2)} \tag{3.4}$$

$$R = (1 - v^2)\lambda^4 + \alpha[(n^2 + \lambda^2)^4 - (2 + v)(3 - v)\lambda^4 n^2 + 2\lambda^4(1 - v^2)$$

$$-\lambda^2 n^4(1 + v) + \lambda^2 n^2(3 + v) + n^4 - 2n^6]$$

$$S = \lambda^2 \begin{Bmatrix} (n^2+\lambda^2)^2 + \frac{2}{1-v}\left(\lambda^2 + \frac{1-v}{2}n^2\right)[1+\alpha(n^2+\lambda^2)^2] \\ -\frac{2v^2\lambda^2}{1-v} + \frac{2\alpha}{1-v}\left(\lambda^2 + \frac{1-v}{2}n^2\right)[n^2+(1-v)\lambda^2 \end{Bmatrix}$$

N_x is the axial load, E is Young's modulus, v is Poisson's ratio, t is the thickness of the thin-walled steel cylindrical tank, and R is the radius of the thin-walled steel cylindrical tank. In Eq. (3.4), the m and n values leading to the buckling stress are unknown until many critical stresses are calculated and compared. The equation requires a lot of calculations of the critical stresses depending on the values of m and n in order to get the lowest critical stress. If many buckling waves are along the length of the thin-walled steel cylindrical tank, the value of λ^2 becomes large. Then, Eq. (3.4) can be simplified as Eq. (3.5).

$$\sigma_{cr} = \frac{N_x}{t} = \frac{1-v^2}{E}\left[\alpha\frac{(n^2+\lambda^2)^2}{\lambda^2} + \frac{(1-v^2)\lambda^2}{(n^2+\lambda^2)^2}\right] \tag{3.5}$$

When the value of n in Eq. (14) is equal to zero, axisymmetric buckling occurs, and Eq. (3.5) can be simplified as Eq. (3.6).

$$\sigma_{cr} = \frac{N_x}{t} = D\left[\frac{m^2\pi^2}{tH^2} + \frac{EH^2}{R^2Dm^2\pi^2}\right] \tag{3.6}$$

where $D = Et^3/[12(1-v^2)]$ is flexural rigidity. Since σ_{cr} is a continuous function of $m\pi/H$, the minimum value of Eq. (3.6) can be written as Eq. (3.7).

$$\sigma_{cr} = \frac{Et}{R\sqrt{3(1-v^2)}} \tag{3.7}$$

The buckling stresses corresponding to the various diameter-to-thickness and height-to-diameter ratios are presented as the ratio of buckling stress to elastic modulus in Table 3.2. The

buckling stresses from numerical analysis are almost the same as the theoretical ones calculated by Eq. (3.7).

Table 3.1. Buckling stresses of the thin-walled steel cylindrical tanks

Models	*H/D*	*D/t*	Buckling Stresses ($\sigma_{cr} \times 10^3/E$)	
			Numerical Analysis	Eq. (16)
A	0.67	910	1.330	1.297
B	2.41	1013	1.195	1.174
C	1.00	1216	0.995	0.973
D	1.46	1612	0.751	0.768
E	0.43	2130	0.568	0.551

3.2.2 Initial Geometric Imperfection

Analytical and experimental research on the static buckling analysis of cylindrical steel structures has been performed. Previous studies focused on the effects of the initial geometric imperfections when the cylindrical steel structures are subjected to the axially compressive loads. Mandra and Mazzolani (1993), using FEM, studied the static behavior of cylindrical shells with diameter-to-thickness ratios less than 400 subjected to axial compression. They found that the static buckling strengths of the thin cylindrical shells were very sensitive to the initial geometric imperfections. The experimental studies were performed to investigate the static buckling behavior of relatively thick cylindrical shells with diameter-to-thickness ratios less than 400 (Donell and Wan, 1950; Miller, 1976; Singer, 1999). Kim and Kim (2002) investigated the buckling strength of the cylindrical shell and tank with diameter-to-thickness ratios of greater than 800 subjected to the axially compressive loads. They found that the buckling strength of the cylindrical shell decreased significantly when the amplitude of initial geometric imperfection increased. The static buckling strength of the cylindrical steel tanks subjected to lateral loads was studied (Roopkumdee

2017; Johnson 2019; Jerath and Lee 2015). They found that the buckling strength decreases significantly as the diameter-to-thickness ratio increases, while it decreases slightly as the height-to-diameter ratio increases.

This chapter aims to study the effect of the initial geometric imperfection on the seismic buckling strength of liquid-filled thin-walled steel cylindrical tanks. To investigate the responses of the initial imperfection thin-walled steel cylindrical tanks to the seismic buckling strength, the first buckling mode shape obtained by eigenvalue analysis was used as the initially imperfect shape of the shell. According to EC3 (2005), if the construction is considered an excellent quality, Eq. (3.8) can be used to indicate the amplitude of initial geometric imperfection.

$$\frac{w_0}{t} = \frac{1}{40}\sqrt{\frac{D}{t}} \tag{3.8}$$

where w_0 is the imperfection amplitude, t is the thickness of the tank, and D is the diameter of the tank.

3.3 Imperfect Geometrical Liquid-Filled Thin-Walled Steel Cylindrical Tanks

Three different earthquakes were included in this study. These three earthquakes have different dynamic characteristics in terms of the time history of acceleration. the El Centro, Parkfield, and Northridge earthquakes are presented in terms of numerical values in the unit of g, the accelerations due to gravity.

3.3.1 El Centro Earthquake

Results show that the imperfection in geometry significantly affects the seismic buckling capacity of the thin-walled steel cylindrical tank. The pseudo-equilibrium paths of initial imperfect geometric tanks are represented as in Fig. 3.2. Transient response in terms of nodal displacement with an increase in PGA is also observed in this study. Fig. 3.3 shows the significant jump in the

nodal displacement of model C which indicates that the structure is unstable for PGA = 0.6g. The node which gave the maximum displacement of each model is used to find the pseudo-equilibrium path. For example, for model C, node 5580 has maximum displacement when PGA is 0.6g as illustrated in Fig. 3.4. For model E, node 1959 has maximum displacement when PGA = 0.1g as illustrated in Fig. 3.5.

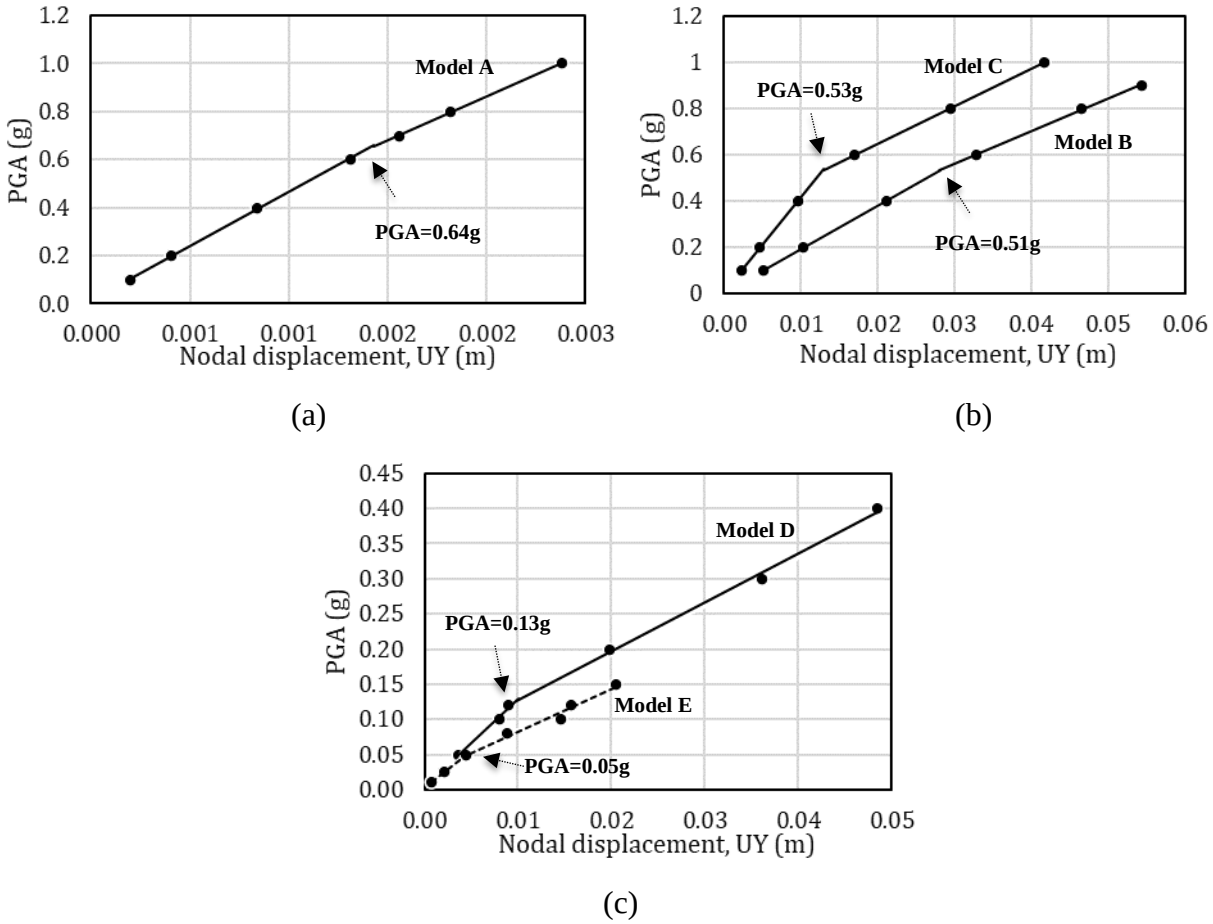

Fig. 3.2. Pseudo-equilibrium paths with initial geometric imperfection; (a) model A, (b) models B and C, (c) models D and E.

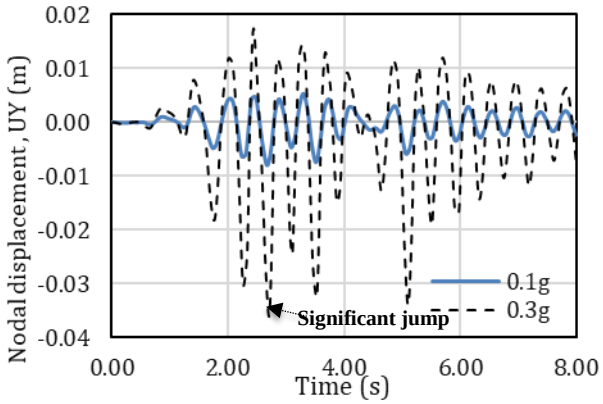

Fig. 3.3. Transient response for model D with initial geometric imperfection.

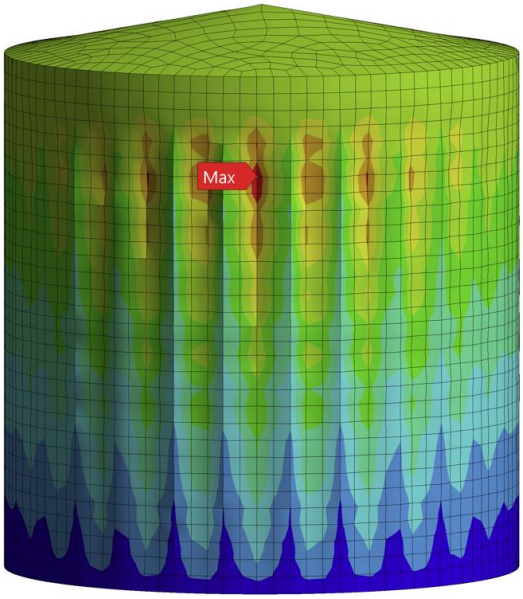

Fig. 3.4. Deformation of model C at PGA = 0.6g, Node 5580.

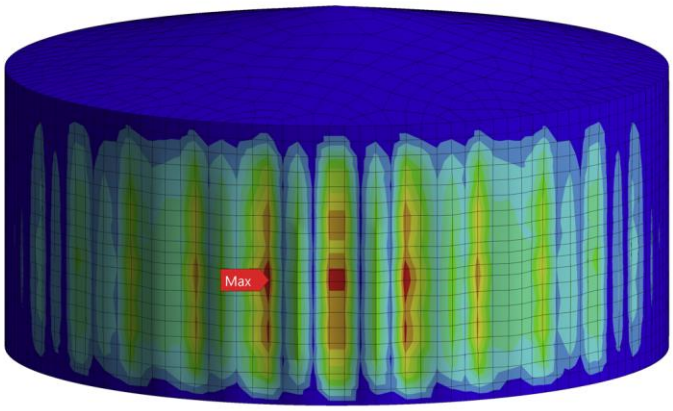

Fig. 3.5. Deformation of model E at PGA = 0.1g, Node 1959.

3.3.2 Parkfield Earthquake

The seismic buckling strengths of the tanks decrease in the range between 7% to 27% when the initial imperfect geometries are considered. The pseudo-equilibrium paths of initial imperfect geometric tanks are represented as in Fig. 3.6. The node which gave the maximum displacement of each model was used to find the pseudo-equilibrium path. Fig. 3.7 shows the example of the maximum displacement of model A when it was subjected to the Parkfield earthquake at PGA = 0.105g, and the maximum displacement occurs at node 2623. Fig. 3.2 shows the example of the maximum displacement of model D when it was subjected to the Parkfield earthquake at PGA = 0.35g, and the maximum displacement occurs at node 1076.

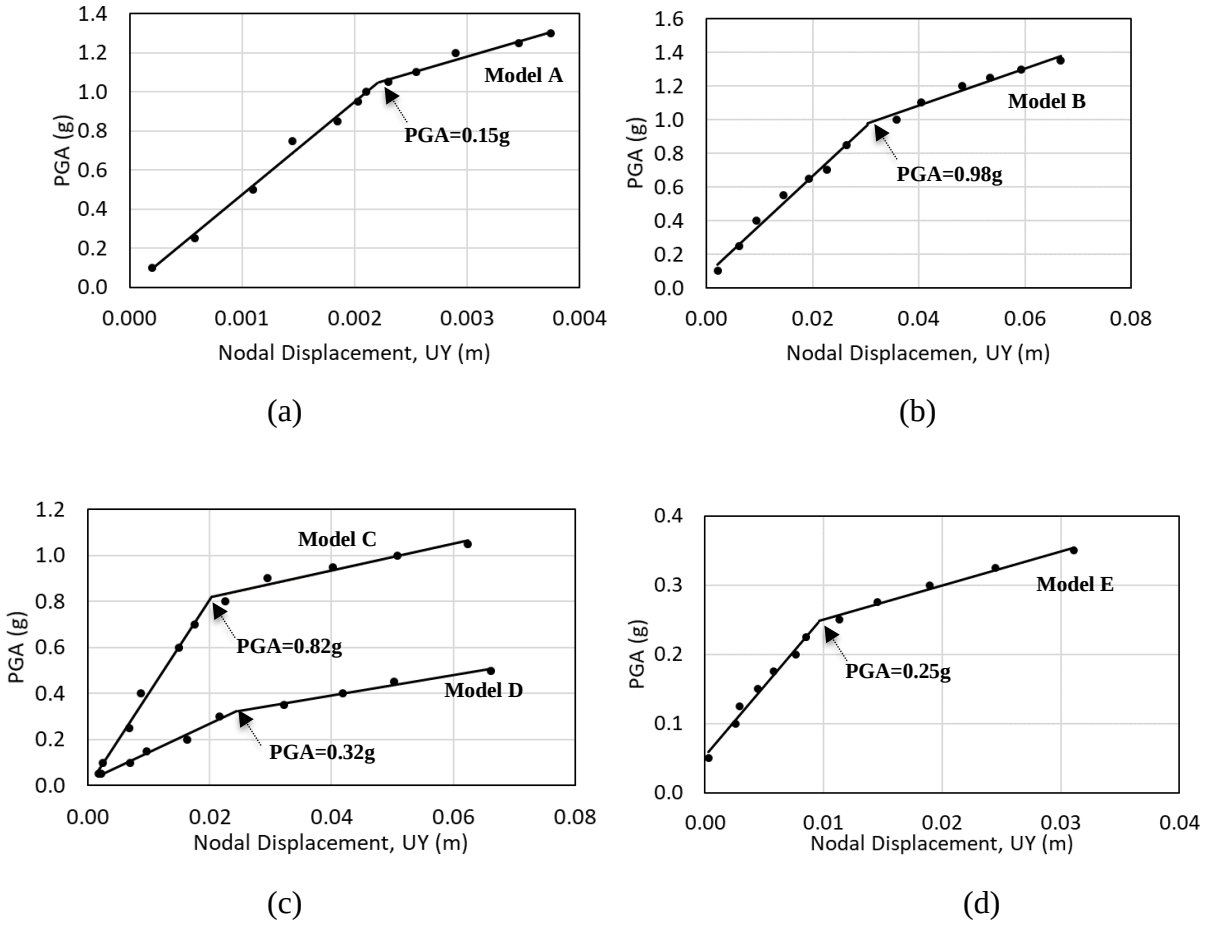

Fig. 3.6. Pseudo-equilibrium paths with initial geometric imperfection; (a) model A, (b) model B, (c) models C and D, and (d) model E.

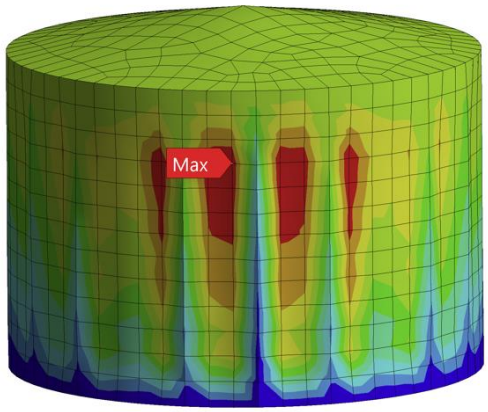

Fig. 3.7. Deformation of model A at PGA = 0.105g, Node 2623.

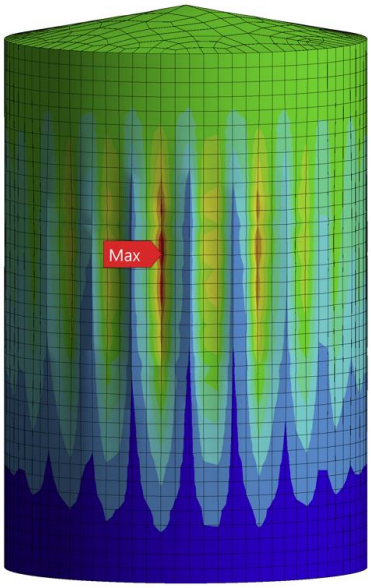

Fig. 3.8. Deformation of model D at PGA = 0.35g, Node 1076.

3.3.3 Northridge Earthquake

The seismic buckling strengths of the tanks decrease in the range between 5% to 25% when the initial imperfect geometries were considered. The pseudo-equilibrium paths of initial imperfect geometric tanks are represented as in Fig. 3.9. The node which gave the maximum displacement of each model was used to find the pseudo-equilibrium path. Fig. 3.10 shows the example of the maximum displacement of model A when it is subjected to the Northridge earthquake at PGA = 1.30g, and the maximum displacement occurs at node 2886. Fig. 3.11 shows the example of the maximum displacement of model E when it is subjected to the Northridge earthquake at PGA = 0.165g, and the maximum displacement occurs at node 2017.

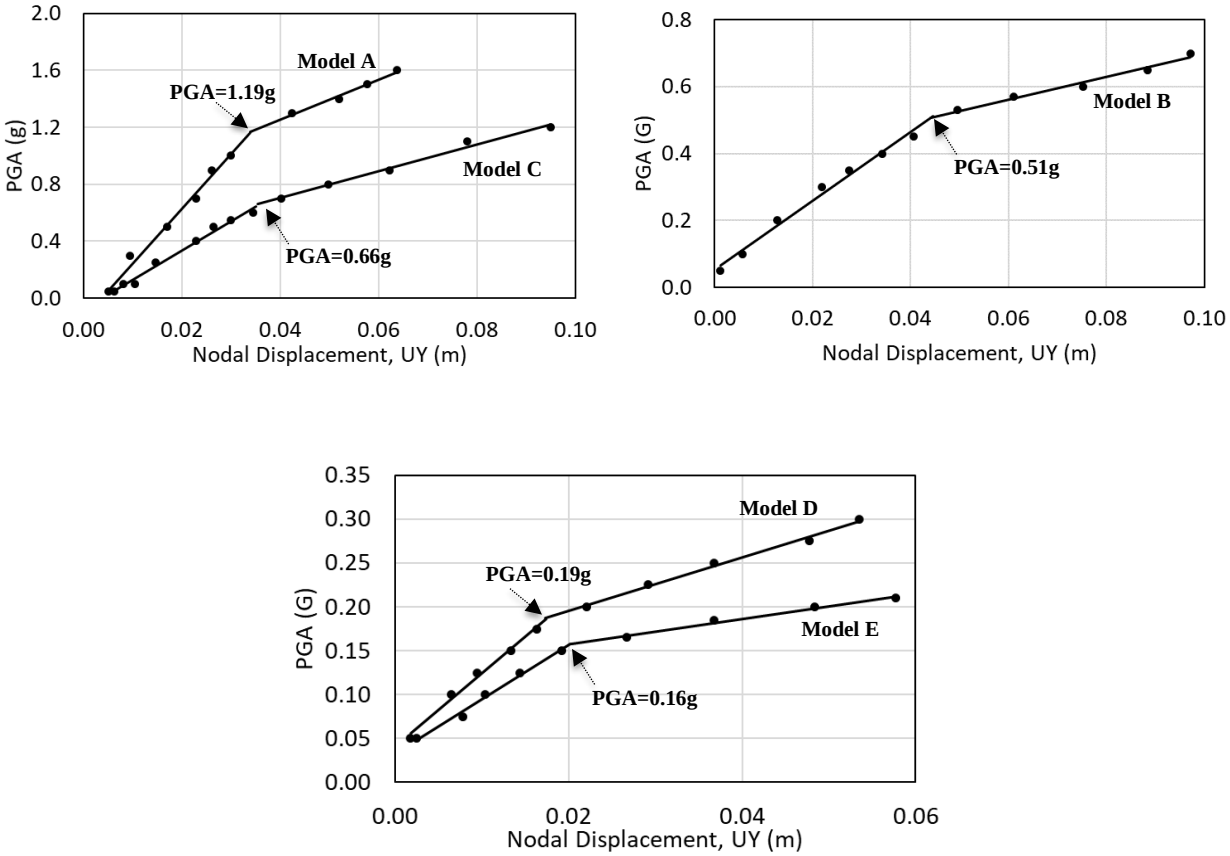

Fig. 3.9. Pseudo-equilibrium paths with initial geometric imperfection; (a) models A and C, (b) model B, and (c) models D and E.

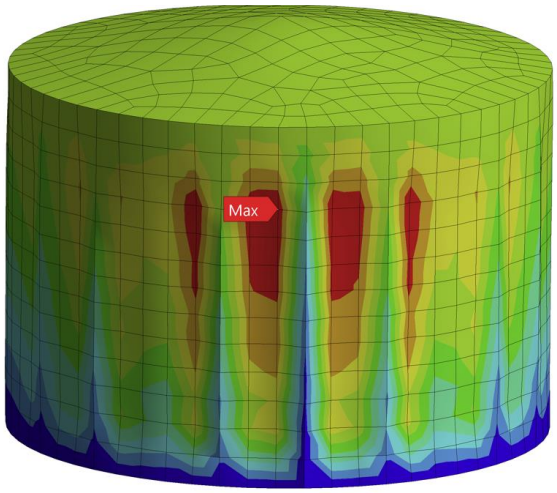

Fig. 3.10. Deformation of model A at PGA = 1.30g, Node 2886.

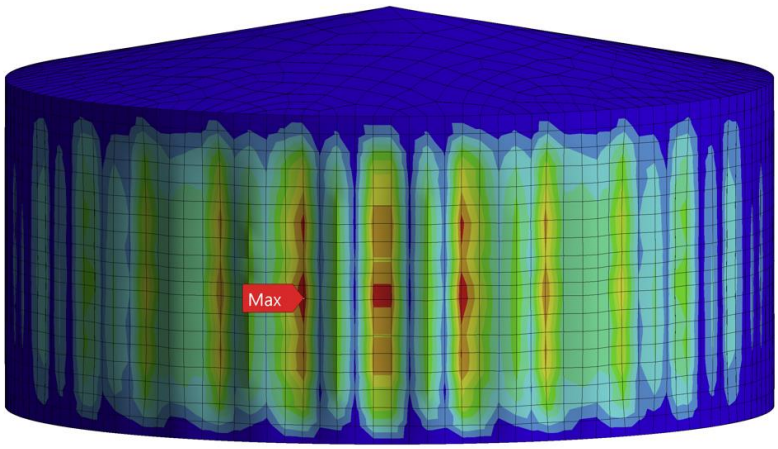

Fig. 3.11. Deformation of model E at PGA = 0.165g, Node 2017.

3.4 Proposed Design Equation

The seismic buckling capacities in terms of PGA for both perfect geometrical and initial imperfect geometrical liquid-filled thin-walled steel cylindrical tanks are listed in Table 3.2.

Table 3.2. Seismic buckling capacities

Model	*H/D*	*D/t*	Seismic Buckling Capacities (PGA), g					
			El Centro		Parkfield		Northridge	
			Perfect	Imperfect	Perfect	Imperfect	Perfect	Imperfect
A	0.67	910	0.72	0.64	1.30	1.05	1.34	1.19
B	2.41	1013	0.55	0.51	1.20	0.98	0.63	0.51
C	1.00	1216	0.56	0.53	0.88	0.82	0.70	0.66
D	1.46	1612	0.15	0.13	0.40	0.32	0.21	0.19
E	0.43	2130	0.075	0.05	0.33	0.25	0.20	0.16

Nonlinear regression analysis was adopted in this study to develop the proposed design equation for the initial geometric imperfect tanks. The proposed design equation for the initial imperfect geometrical liquid-filled thin-walled steel cylindrical tank steel tanks is estimated as Eq. (3.9).

$$PGA = -0.2248\ln(H/D) - 1.009(10)^{-4}(D/t)^{1.25} + 1.392 \quad (3.9)$$

R^2 value of Eq. (3.9) is 0.7679. The coefficients of *D/t* and *H/D* ratios are statistically significant at a 95% confident interval. By comparing Eq. (3.9) to Eq. (2.9), it can be concluded that the seismic buckling of the liquid-filled thin-walled steel cylindrical tank decreases significantly if there is initial geometric imperfection. For the interaction effect between *D/t* and *H/D* ratios on *PGA, the D/t* ratio has a significant negative effect on the seismic buckling capacity. If the *D/t* ratio increases, the seismic buckling capacity will significantly decrease. An increase in the *H/D* ratio also shows a negative effect on seismic buckling capacity; however, it is less significant than the *D/t* ratio.

3.5 Summary

This chapter aims to evaluate the effect of the initial geometric imperfection of the liquid-filled thin-walled steel cylindrical tanks on seismic buckling strength. The effects of *D/t*, *H/D* ratios, and initial geometric imperfection on the dynamic buckling were investigated, and an estimated design equation was proposed. From this study, the following conclusions are drawn:

- The geometric imperfection is an important factor that can reduce the seismic buckling strength of the liquid-filled thin-walled steel cylindrical tanks. This study found that initial geometric imperfection significantly reduces the seismic buckling capacity in the range between 5% to 33%.

- Similar to the seismic behavior of geometric perfect tanks, the *D/t* ratio is an important parametric factor of the seismic buckling strength of the liquid-filled thin-walled steel cylindrical tank. The seismic buckling capacity of the tank decreases significantly when the *D/t* ratio increases. An increase in the *H/D* ratio decreases the seismic buckling capacity of the tank; however, its effect is less significant compared to the D/t ratio.

CHAPTER 4 Seismic Buckling Evaluation of Stiffened Liquid-Filled Thin-Walled Steel Cylindrical Tanks

4.1 Introduction

This chapter aims to investigate the seismic buckling strength of unstiffened and stiffened liquid-filled thin-walled steel cylindrical tanks under horizontal earthquake excitation. Seismic buckling behaviors of the stiffened and unstiffened liquid-filled thin-walled steel cylindrical tanks under seismic load have been investigated in previous literature. Some researchers studied the grouping effect of the storage tanks on seismic buckling strength (Burgos et al., 2015; Portela and Godoy, 2005; Sabransky and Melbourne, 1987; Kebeli, 2002). They found that the grouping effect of storage tanks is another important factor in studying the seismic buckling behaviors. The seismic responses of the cylindrical shell structures have been investigated (Zhao and Lin, 2014; Uematsu et al., 2014; Yasunaga et al., 2012a; 2012b; Resinger and Greiner, 1982). Sun et al. (2018) studied the stability of open-topped storage tanks with top stiffener and one intermediate stiffener subjected to wing loading. They found that the cylindrical storage tank only needs one intermediate stiffener ring, the size of the top stiffener ring can be set to the same size as the intermediate stiffener ring. However, the knowledge of the seismic buckling behaviors of the liquid-filled thin-walled steel cylindrical tanks with vertical stiffeners subjected to different earthquake excitation is very limited. Therefore, the seismic buckling behaviors of stiffened liquid-filled thin-walled steel cylindrical tanks under earthquake excitations were studied using FEM in this chapter.

Ten finite element models of liquid-filled thin-walled steel cylindrical tanks with diameter-to-thickness ratios (D/t) ratios of 910, 1013, 1216, 1612, and 2130 and the height-to-diameter (H/D) ratios of 0.43, 0.67, 1.00, 1.46, and 2.41 were used to investigate the buckling behaviors of various sizes of the thin-walled steel cylindrical tanks under earthquake excitation. Four vertical

stiffeners around the circumference were included for stiffened thin-walled steel cylindrical tanks. The transient analyses were carried out using a commercial finite element program ANSYS. Pseudo-Equilibrium path and phase plane criterion were used to evaluate the seismic buckling strength. According to the results of both unstiffened and stiffened liquid-filled thin-walled steel cylindrical tanks, the seismic buckling strength decreases significantly as the diameter-to-thickness (*D/t*) ratio increases, while it decreases slightly as the height-to-diameter (*H/D*) ratio increases. The results show that the vertical stiffeners can improve the seismic buckling strength by at least around 10% of the critical peak ground acceleration (PGA) compared to the unstiffened liquid-filled thin-walled steel cylindrical tanks. Based on the extensive parametric study, the interaction effects of *D/t* ratio, *H/D* ratio, and vertical stiffener for the liquid-filled thin-walled steel cylindrical tanks of various geometries subjected to the El Centro 1940 earthquake are presented and discussed.

4.2 Methodology

4.2.1 Numerical Models

Ten different geometrical configurations of the liquid-filled thin-walled steel cylindrical tanks are analyzed with height-to-diameter (H/D) ratios of 0.43, 0.67, 1.00, 1.46, and 2.41 and the diameter-to-thickness (D/t) ratios of 910, 1013, 1216, 1612, and 2130 to investigate the buckling behaviors of various sizes of the liquid-filled thin-walled steel cylindrical tanks. The geometries of the liquid-filled thin-walled steel cylindrical tanks are shown in Table 4.1. The unstiffened liquid-filled thin-walled steel cylindrical tanks are represented as tank A, B, C, D, and E, and the liquid-filled thin-walled steel cylindrical tanks with vertical stiffeners are represented as tank AS, BS, CS, DS, and ES, respectively. The material properties of structural steel and liquid-filled

inside the thin-walled steel cylindrical tanks are identical to the material properties as discussed in section 2.2.1.

Table 4.1. Geometries of the cylindrical tanks

Tank	H (m)	D (m)	t (mm)	H_r (m)	H/D	D/t	Stiffeners
A	6.1	9.1	10.0	0.853	0.67	910	-
AS	6.1	9.1	10.0	0.853	0.67	910	Vertical stiffeners
B	18.3	7.6	7.5	0.713	2.41	1013	-
BS	18.3	7.6	7.5	0.713	2.41	1013	Vertical stiffeners
C	15.2	15.2	12.5	1.425	1.00	1216	-
CS	15.2	15.2	12.5	1.425	1.00	1216	Vertical stiffeners
D	20.0	13.7	8.5	1.284	1.46	1612	-
DS	20.0	13.7	8.5	1.284	1.46	1612	Vertical stiffeners
E	9.1	21.3	10.0	2.000	0.43	2130	-
ES	9.1	21.3	10.0	2.000	0.43	2130	Vertical stiffeners

The liquid-filled thin-walled steel cylindrical tanks with four vertical stiffeners around the circumference were included in this study to investigate the mode shapes and development of seismic buckling capacities of the liquid-filled thin-walled steel cylindrical tanks. The material properties of stiffeners are the same as the liquid-filled thin-walled steel cylindrical tanks. The thicknesses of stiffeners are equal to the thicknesses of the liquid-filled thin-walled steel cylindrical tanks, with widths of stiffeners equal to 15 cm for every tank. The lengths of stiffeners are equal to the heights of the liquid-filled thin-walled steel cylindrical tanks. SHELL 181 is used to be the element for stiffeners. Stiffeners for the liquid-filled thin-walled steel cylindrical tanks A, B, C, D, and E are modeled with 812, 2436, 2023, 2662, and 1211 SHELL181 elements, respectively. Fig. 4.1 represents the finite element meshing of tank AS.

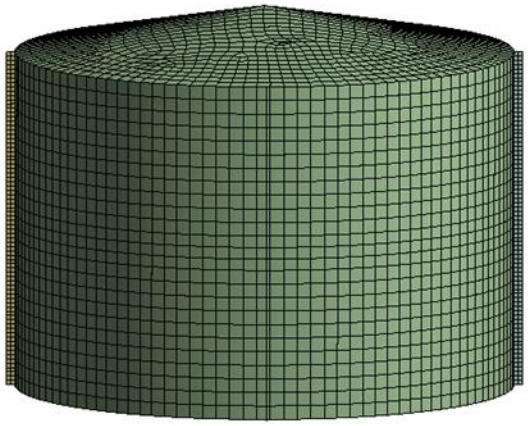

Fig. 4.1. Finite element meshing of the steel cylindrical tanks AS.

4.2.3 First Natural Frequencies and Damping Ratios

Results from the modal analysis show that the natural frequencies increase, and the first mode shapes also change when the liquid-filled thin-walled steel cylindrical tanks are stiffened by vertical stiffeners. The increases of the first natural frequencies are represented in Table 4.2. Fig. 4.2 illustrates the first mode shapes of tanks A and AS. Figs. 4.3 illustrates changes in the first mode shapes of tanks D and DS. The natural frequencies and mode shapes are the parameters that are used to find mass coefficients for the Rayleigh damping method in the transient analysis. Table 4.3 shows the calculated mass coefficients (a_0) for the unstiffened and stiffened liquid-filled thin-walled steel cylindrical tanks.

Table 4.2. First natural frequencies

Tank	1st Natural frequencies (Hz)
A	4.259
AS	4.920
B	1.993
BS	3.665
C	2.293
CS	2.528
D	1.824
DS	2.745
E	2.070
ES	2.433

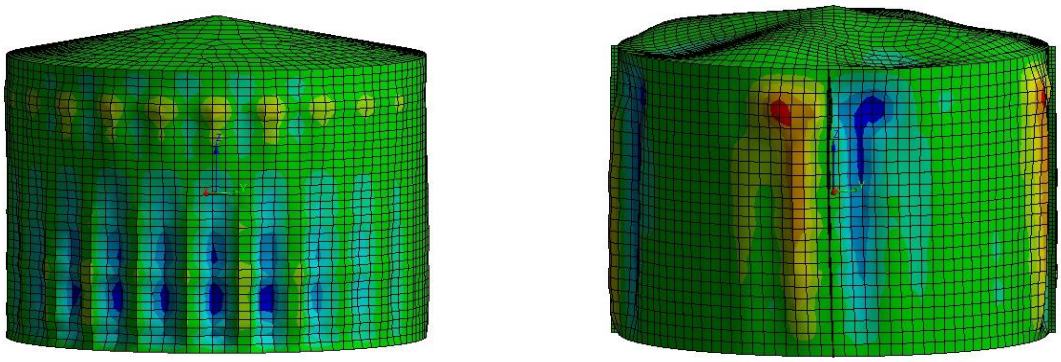

Fig. 4.2. First natural mode shapes: (a) tanks A; (b) tank AS.

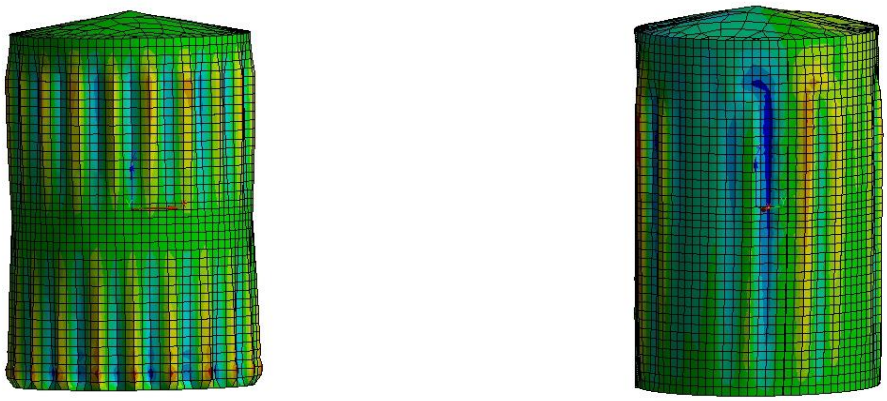

Fig. 4.3. First natural mode shapes: (a) tank D, (b) tank DS.

Table 4.3. Mass coefficients

Tank	**Mass coefficient (a_0)**
A	1.070
AS	1.237
B	0.501
BS	0.921
C	0.576
CS	0.635
D	0.458
DS	0.690
E	0.520
ES	0.611

4.3 Seismic Buckling Analysis

4.3.1 Buckling Criterions

The Budiansky and Roth criterion (1962) was employed in this study, as it has been broadly used as a technique to determine the dynamic buckling load of structures. This criterion is based

on a significant jump in displacement responding to an increase in load; therefore, several analyses need to be conducted using different loads. The plots of the peak displacements responding to the applied loads are obtained according to Budiansky and Roth criterion, which has been mentioned as the "pseudo-equilibrium path" in this study. However, due to the seismic nature of earthquake loads, if the loading is not maintained long enough in its direction to produce a high jump, seismic buckling is sometimes difficult to identify (Virella, 2006).

Phase plane criterion was used as a second verification to determine the seismic buckling of the structures in this study since seismic buckling is sometimes difficult to identify using the Budiansky and Roth criterion. The phase plane criterion is a graphical method that represents a change in the possible state of the system with times (Singiresu, 1995). The phase plane curve illustrates the movement between the displacement and velocity of interested nodes. For the stable state, the curve does not move away from the static equilibrium which is located at the center of the attraction. However, when the load reaches an unstable state, the curve will move away from the pole of the attraction. Previous research used a phase plane criterion to identify the dynamic buckling of the structures (Roopkumdee and Mamaghani 2019; Auli and Rammerstorfer, 1986; Djermane 2014; Hjelmstad and Williamson, 1988).

4.3.2 Unstiffened Liquid-Filled Thin-Walled Steel Cylindrical Tanks

The nonlinear transient analyses of unstiffened liquid-filled thin-walled steel cylindrical tanks are performed to investigate the seismic buckling capacities and the interaction effects between *D/t* and *H/D* ratios. The location of elements where the maximum radial displacement occurs is tracked for every single tank. The tracked elements are used to find the significant jump of the radial displacement when the PGA is increased. Figs. 4.4(a) and (b) show the location of buckling zones when tanks C and E are subjected to PGAs of the El Centro earthquake of 0.6g and

0.1g, respectively. The differences in D/t and H/D ratios can affect the seismic buckling zones of the liquid-filled thin-walled steel cylindrical tanks. The buckling zones occur slightly below the top of tank C and slightly below the middle of the height of tank E, as can be seen in Fig. 4.4(a) and (b).

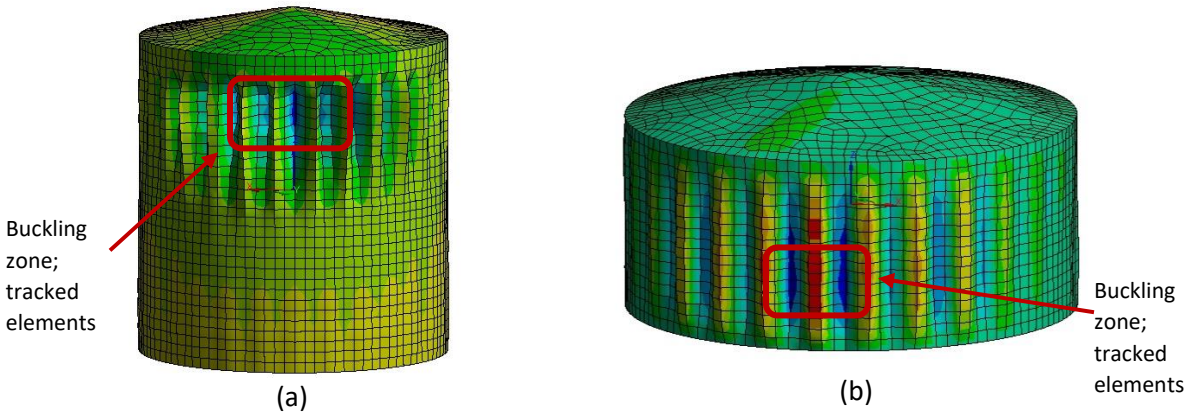

Fig. 4.4. Radial displacement: (a) tank C at 0.6g; (b) tank E at 0.1g.

The response of radial displacement due to an increase of PGA value can be illustrated as the transient response curve. The significant jump of displacement can be observed when the observed point structure moves from a stable to an unstable system. Fig. 4.4 shows the significant jumps of tanks A and C when the systems of these two models change from stable to unstable. For example, in Fig. 4.5(b), the PGA changes from 0.30g to 0.60g, and the response of radial displacement change significantly from 0.00256 m to 0.0083 m.

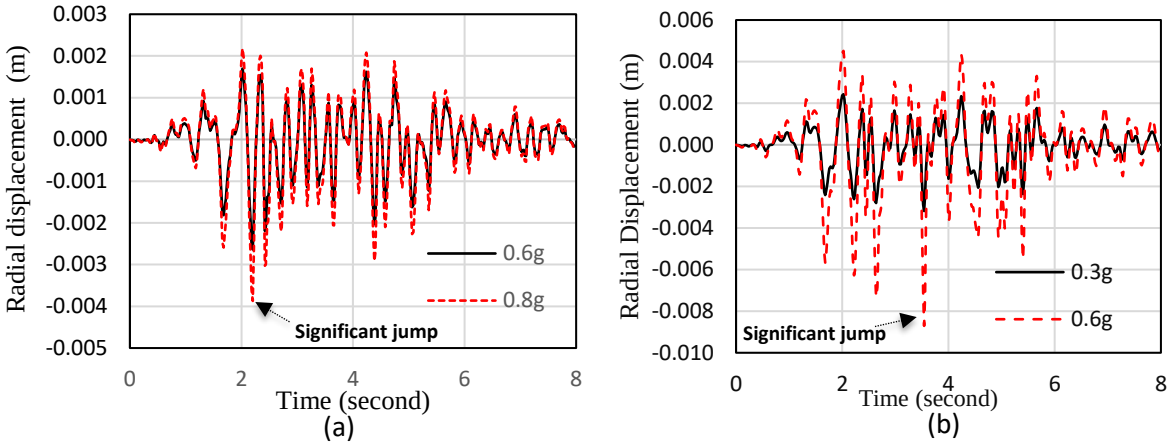

Fig. 4.5. Transient responses: (a) tank A; (b) tank C

Fig. 4.6. shows the pseudo-equilibrium paths and the significant jumps of unstiffened liquid-filled thin-walled steel cylindrical tanks. The seismic buckling capacities can be observed from a change in the slope of curves as shown in Fig. 8. The seismic buckling capacities for the liquid-filled thin-walled steel cylindrical tanks A, B, C, D, and E are equal to 0.72g, 0.55g, 0.56g, 0.15g, and 0.075g, respectively. The phase plane curves are generated to verify if the results from the pseudo-equilibrium paths are accurate because the significant jump in displacement is sometimes difficult to observe. Tanks B and D show uncertain displacement jumps as shown in Fig. 4.6(b) and (c). Therefore, the buckling capacities of tanks B and D were reinvestigated using phase plane criterion to examine the movements of displacement-velocity curves for pre-buckling and post-buckling PGAs as shown in Figs. 4.7 and 4.8, respectively.

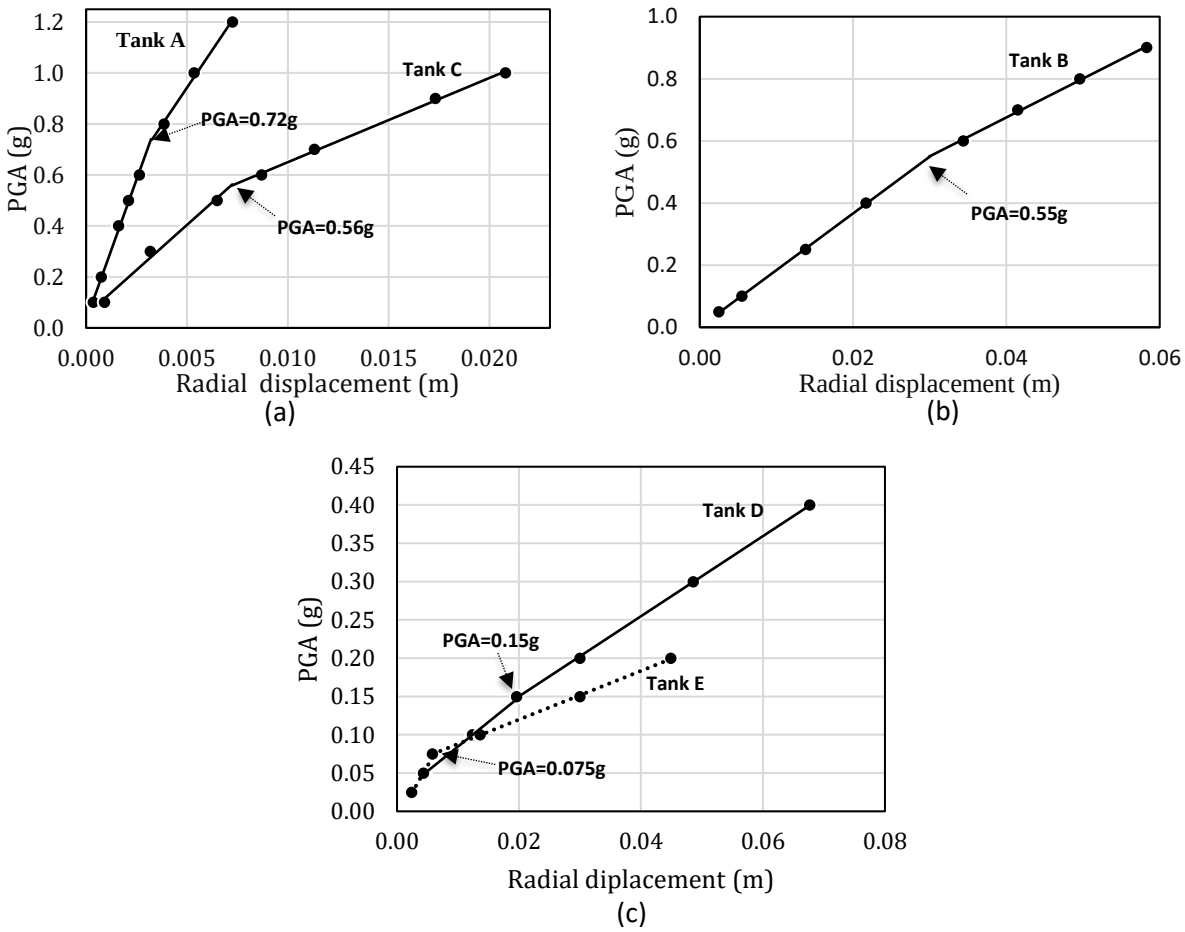

Fig. 4.6. Pseudo-equilibrium paths for unstiffened liquid-filled thin-walled steel cylindrical tanks: (a) tanks A and C; (b) tank B; (c) tanks D and E.

Figs. 4.7(a) and 4.8(a) represent the movements of displacement-velocity curves that tend to move around the origin point (0, 0). On the other hand, Figs. 4.7(b) and 4.8(b) represent the movements of displacement-velocity curves that seem to move away from the origin point (0, 0) compared to Figs. 4.7(a) and 4.8(a), respectively. Figs. 4.7 and 4.8 can be used to prove that the seismic buckling capacities of tanks B and D when they are subjected to the El Centro earthquake are between 0.40g to 0.60g and 0.10g to 0.20g, respectively.

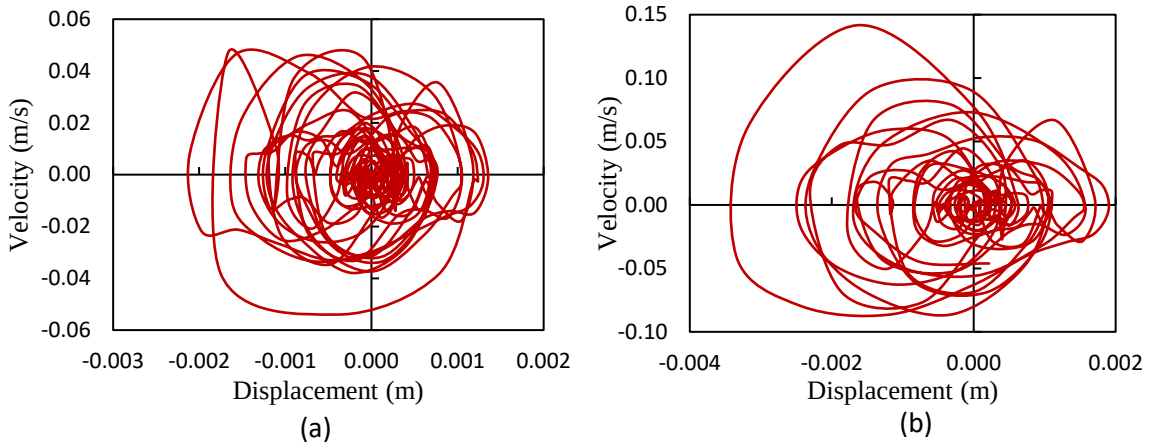

Fig. 4.7. Phase plane curves of tank B (a) pre-buckling at PGA = 0.40g (b) post-buckling at PGA = 0.60g

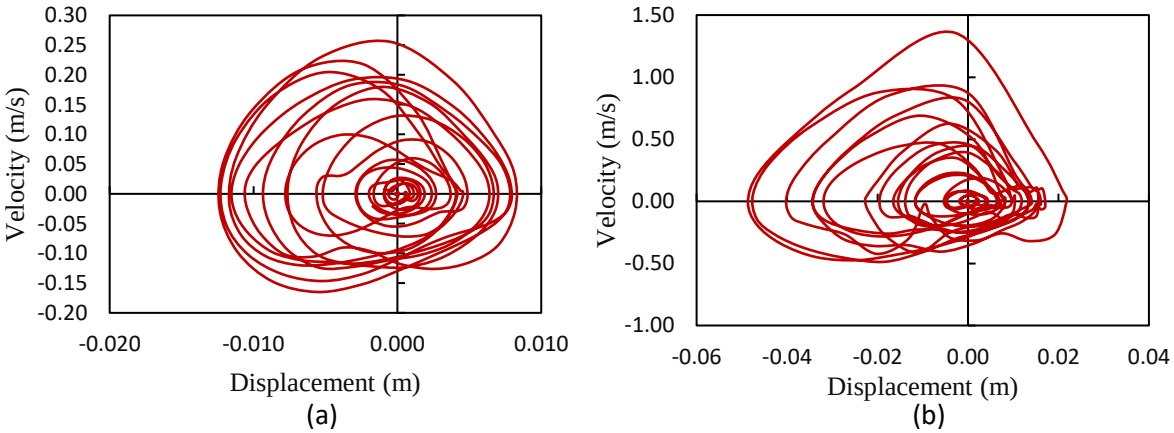

Fig. 4.8. Phase plane curves of tank D (a) pre-buckling at PGA = 0.10g (b) post-buckling at PGA = 0.20g

The von-Mises stresses at the PGAs which are slightly above the critical PGAs for the unstiffened liquid-filled thin-walled steel cylindrical tanks are represented in Table 4.4. The von-Mises stresses at the first instability points do not reach the yield stress for any tank since the yield stress in this study is assumed to be 345 MPa, which is equal to ASTM A572 steel (ASTM, 2018). Therefore, all buckling cases for unstiffened liquid-filled thin-walled steel cylindrical tanks are elastic buckling. Figs. 4.9(a) and 4.9(b) show the maximum von-Mises stresses of the first instability at the buckling zone of tanks C and D, respectively.

Table 4.4. Post-buckling von-Mises stresses for unstiffened liquid-filled thin-walled steel cylindrical tanks.

Tank	D/t	H/D	PGA (g)	von-Mises stress (MPa)
A	910	0.67	0.80	84.65
B	1,013	2.41	0.60	200.51
C	1,216	1.00	0.60	270.68
D	1,612	0.15	0.15	108.58
E	2,130	0.10	0.10	94.13

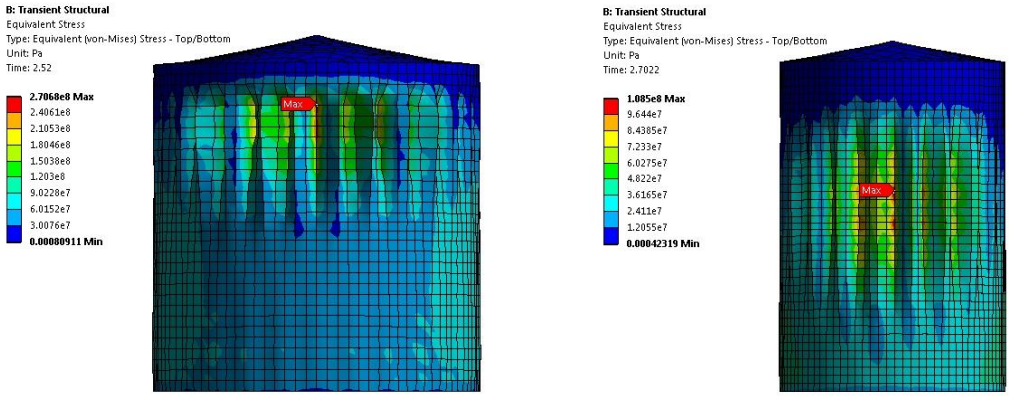

(a) (b)

Fig. 4.9. von-Mises stress after buckling: (a) tank C; (b) tank D

4.3.3 Stiffened Liquid-Filled Thin-Walled Steel Cylindrical Tanks

This study investigated the development of seismic buckling capacity due to vertical stiffeners. The material properties and geometries of the stiffeners were discussed in section 4.2.1. Both Budiansky and Roth criterion and phase plane curve were used to estimate the seismic buckling capacities of the stiffened liquid-filled thin-walled steel cylindrical tanks are adopted in this section. Figs. 4.10(a) and (b) show the locations of buckling zones when tanks AS and DS were subjected to PGAs of the El Centro earthquake of 0.95g and 0.25g, respectively. Fig. 4.11 shows the transient responses and the significant jumps in radial displacements of tanks BS and ES. The first significant jump in radial displacement for tank ES can be observed when the PGAs

are higher than 0.15g as shown in Fig. 4.11(b). Fig. 4.11(b) represents that the seismic buckling of tank ES should be higher than 0.15g, which means that the vertical stiffeners can improve the seismic buckling capacity.

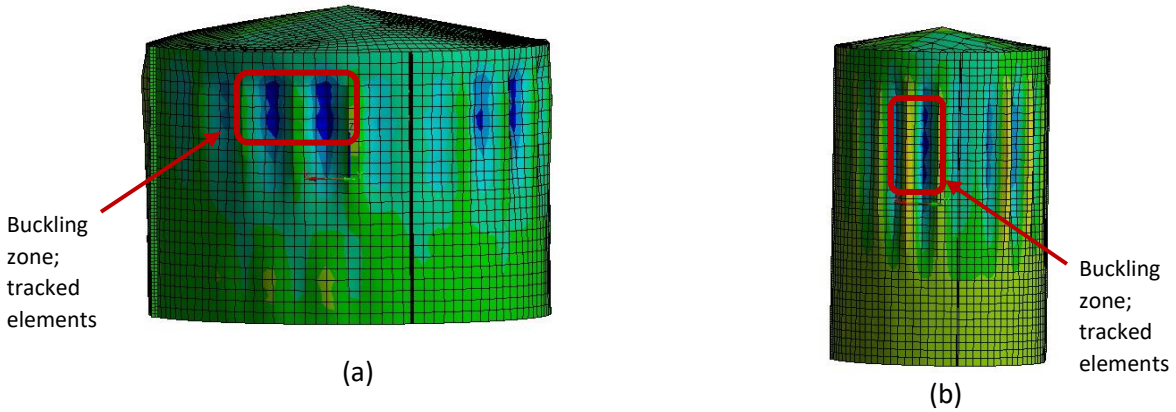

Fig. 4.10. Radial displacement: (a) tank AS at 0.95g; (b) tank DS at 0.25g

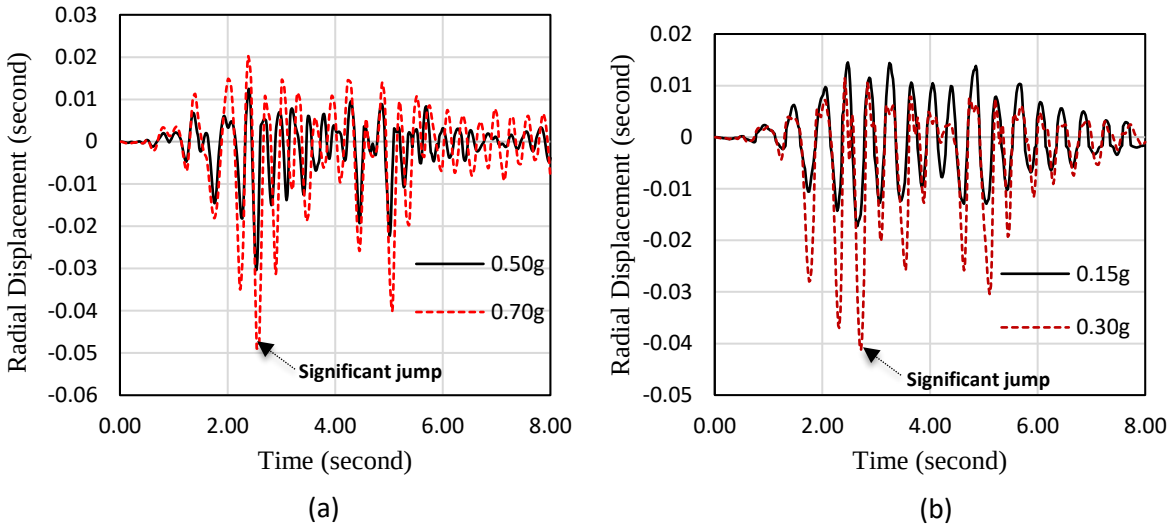

Fig. 4.11. Transient response: (a) tank BS; (b) tank ES

Fig. 4.12. shows the pseudo-equilibrium paths and the significant jumps of stiffened liquid-filled thin-walled steel cylindrical tanks. The seismic buckling capacities for tanks AS, BS, CS, DS, and ES are equal to 0.85g, 0.61g, 0.63g, 0.23g, and 0.18g, respectively. The seismic buckling capacities of stiffened liquid-filled thin-walled steel cylindrical tanks are higher than

the seismic buckling capacities of unstiffened liquid-filled thin-walled steel cylindrical tanks. By comparing Fig. 4.6 and Fig. 4.12, the seismic buckling capacities increase for every model when the stiffeners are included. The improvements of the seismic buckling capacity of the liquid-filled thin-walled steel cylindrical tanks are listed in Table 4.6.

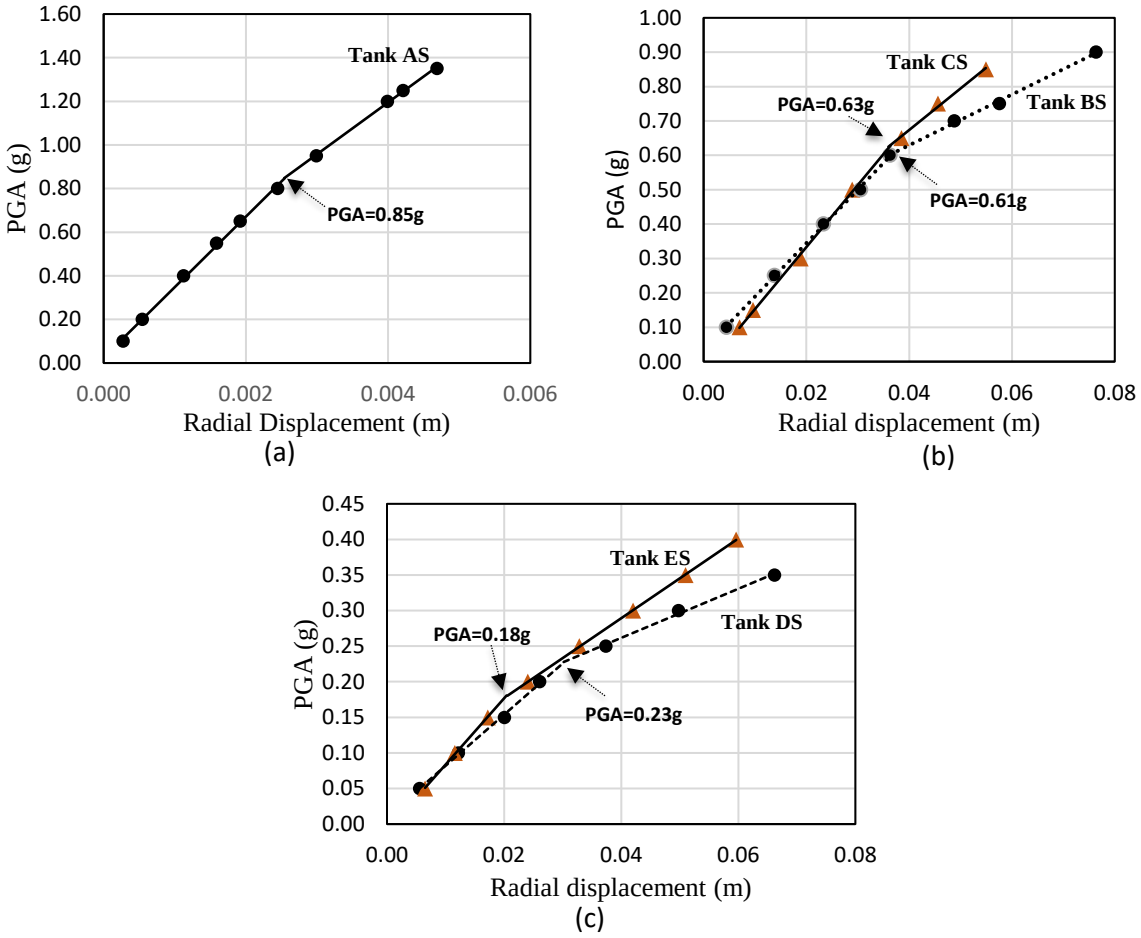

Fig. 4.12. Pseudo-equilibrium paths: (a) tank AS; (b) tanks BS and CS; (c) tanks DS and ES

Phase plane curves are performed to reinvestigate the buckling capacities of tanks AS and CS because the pseudo-equilibrium paths of tanks AS and CS show slight changes in slopes, as can be seen in Fig. 4.12. Figs. 4.13 and 4.14 show the phase plane curves for tanks AS and CS, respectively. Figs. 4.13 and 4.14 can be used to prove that the seismic buckling capacities of tanks

AS and CS when they are subjected to the El Centro earthquake are between 0.80g to 0.95g and 0.50g to 0.65g, respectively.

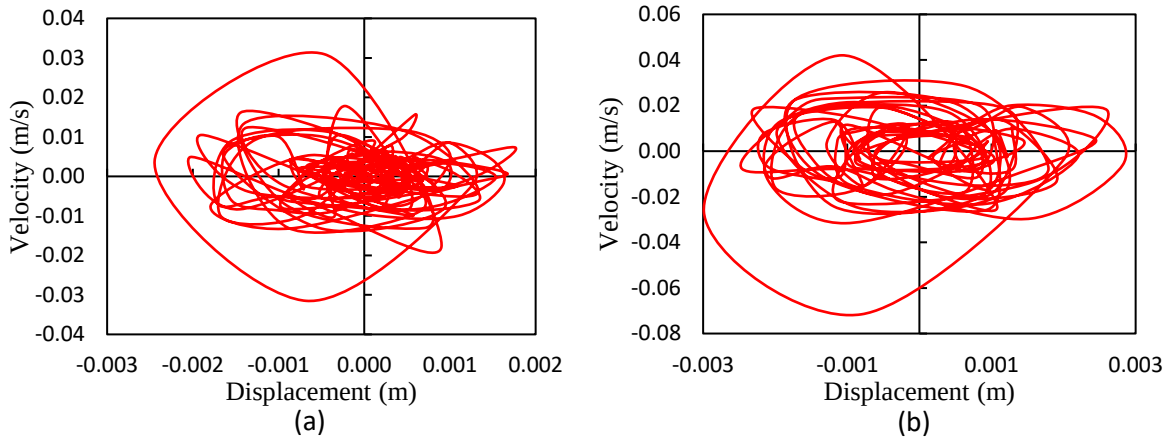

Fig. 4.13. Phase plane curves of tank AS: (a) PGA = 0.80g; (b) PGA = 0.95g

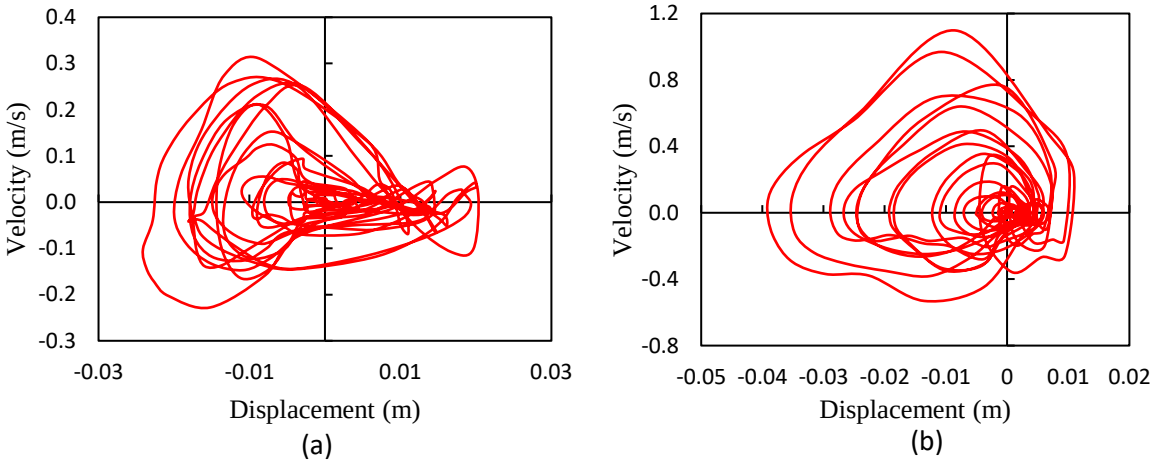

Fig. 4.14. Phase plane curves of tank CS: (a) PGA = 0.50g; (b) PGA = 0.65g

The von-Mises stresses at the PGAs, which are slightly above the critical PGAs for the stiffened liquid-filled thin-walled steel cylindrical tanks, are represented as in Table 4.5. The von-Mises stresses at the walls for the first instability points do not reach the yield stress of 345 MPa for any stiffened liquid-filled thin-walled steel cylindrical tanks. The highest von-Mises stress at the first instability point is 282.20 MPa at 0.70g for tank CS. The von-Mises stress at the walls at the first instability points of the stiffened liquid-filled thin-walled steel cylindrical tanks

are slightly higher than unstiffened liquid-filled thin-walled steel cylindrical tanks by comparing Tables 4.4 and 4.5. However, the stiffeners yield at the critical PGAs for every tank except tank AS. The maximum von-Mises stresses usually occur at the base of the stiffeners. Figs. 4.15 and 4.17 show the maximum von-Mises stresses which occur at the base of the vertical stiffeners for tanks BS and ES, respectively. Fig. 4.16 shows the maximum von-Mises stress of the stiffener which occurs slightly below the top of the liquid-filled thin-walled steel cylindrical tanks.

Table 4.5. Post-buckling von-Mises stresses for stiffened liquid-filled thin-walled steel cylindrical tanks.

Tank	D/t	H/D	PGA (g)	Maximum von-Mises stresses at walls (MPa)	Maximum von-Mises stresses at stiffeners (MPa)
AS	910	0.67	0.95	97.08	108.65
BS	1013	2.41	0.65	249.97	416.09
CS	1216	1.00	0.70	282.20	407.09
DS	1612	1.46	0.25	172.11	464.82
ES	2130	0.43	0.20	145.28	401.27

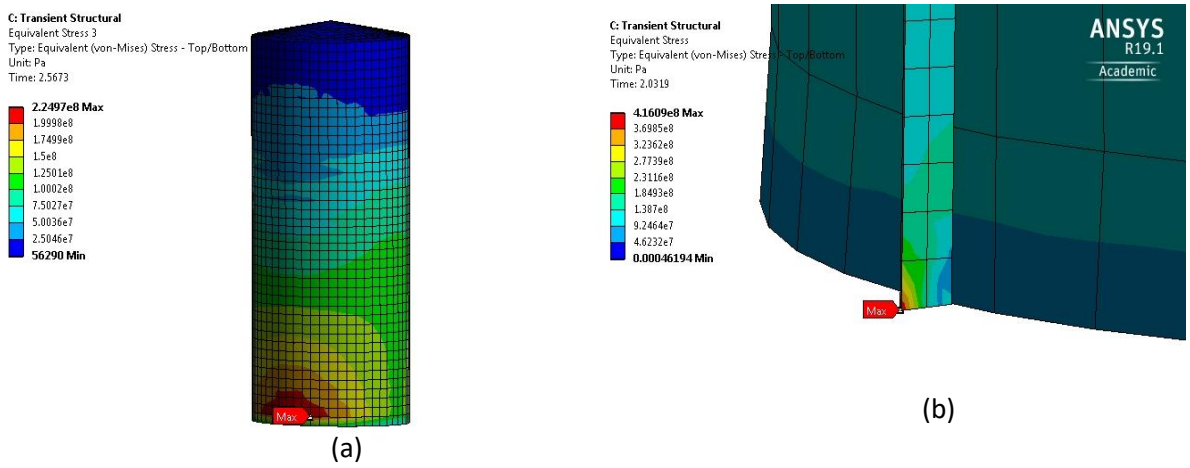

Fig. 4.15. von-Mises stresses of tank BS after buckling: (a) wall stress; (b) stiffeners stress

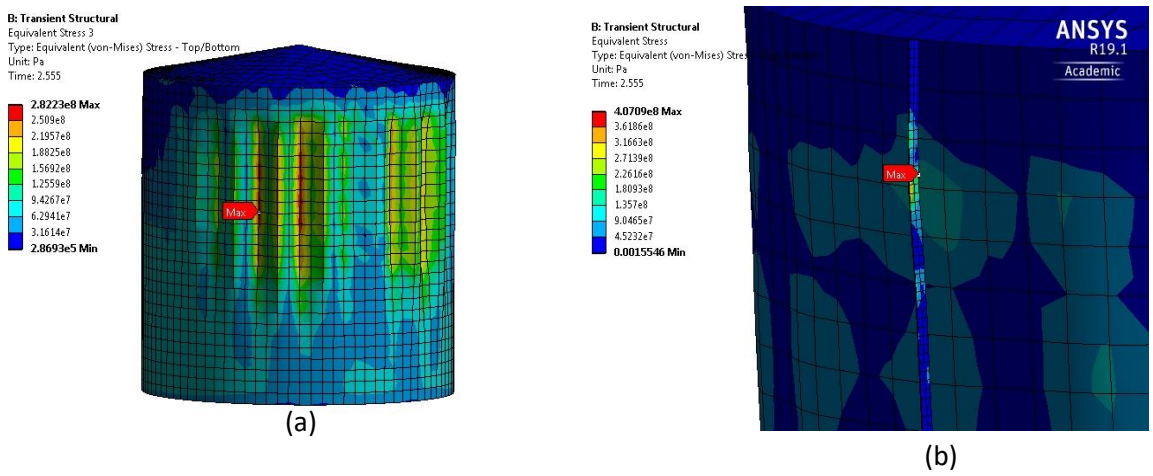

Fig. 4.16. von-Mises stresses of tank CS after buckling: (a) wall stress; (b) stiffeners stress

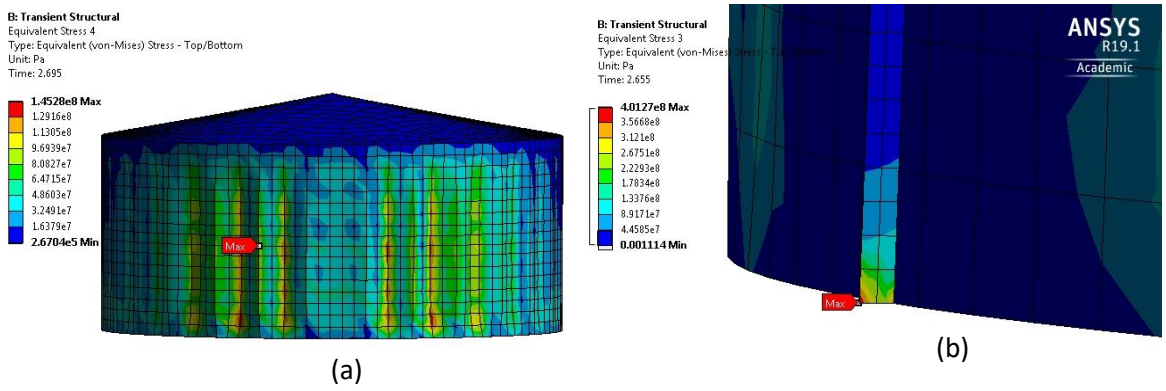

Fig. 4.17. von-Mises stresses of tank ES after buckling: (a) wall stress; (b) stiffeners stress

4.4 Proposed Design Equation

The seismic buckling capacities of unstiffened and stiffened liquid-filled thin-walled steel cylindrical tanks under El Centro earthquake accelerations are presented in Table 4.6. Table 4.6 shows that the seismic buckling capacities of stiffened liquid-filled thin-walled steel cylindrical tanks are higher than the seismic buckling capacities of unstiffened liquid-filled thin-walled steel

cylindrical tanks. The seismic buckling capacities increase at least 10 percent when the vertical stiffeners are included.

Table 4.6. Seismic buckling capacities

Tank	Seismic buckling capacities (g)
A	0.72
AS	0.85
B	0.55
BS	0.61
C	0.56
CS	0.63
D	0.15
DS	0.23
E	0.075
ES	0.18

Nonlinear regression analysis was used to investigate the interaction effects of *D/t* ratios, *H/D* ratios, and vertical stiffeners on seismic buckling capacities. Eq. (4.3) represents the estimations of seismic buckling capacities based on multiple nonlinear regression.

$$PGA = -0.1657\ln(H/D) - 8.28(10^{-5})(D/t)^{1.25} + 0.089(Stiffeners) + 1.1169 \qquad (4.1)$$

where "*Stiffeners"* is a binary regressor; *Stiffeners* = 1 if a tank is stiffened by vertical stiffeners, and *Stiffeners* = 0 if a tank is unstiffened.

R^2 value of Eq. (4.1) is 0.975. The coefficients of *D/t* ratio, *H/D* ratio, and *Stiffeners* are statistically significant at a 95% confident interval. Eq. (4.1) shows that the critical PGA

decreases with the exponential rate when the *D/t* ratio increases and decreases with diminishing rate when the H/D ratio increases. The critical PGA increases when the liquid-filled thin-walled steel cylindrical tanks are stiffened by vertical stiffeners.

4.5 Summary

The interaction effects between *D/t* and *H/D* ratios can affect the seismic buckling capacities of the liquid-filled thin-walled steel cylindrical tanks, and the vertical stiffeners can increase the seismic buckling strength of the cylindrical tanks. Some of the main points are:

1. The vertical stiffeners can improve the seismic buckling strength of liquid-filled thin-walled steel cylindrical tanks when they are subjected to horizontal earthquake excitation. The vertical stiffeners can improve the seismic buckling strength by at least 10% of the critical PGA of unstiffened liquid-filled thin-walled steel cylindrical tanks.
2. For both unstiffened and stiffened liquid-filled thin-walled steel cylindrical tanks, the von-Mises stresses at the buckling zone at the walls of the cylindrical tanks do not reach the yield point at the critical PGAs.
3. The *D/t* ratio is an important parametric factor for the seismic buckling strength of the liquid-filled thin-walled steel cylindrical tank. The seismic buckling capacities of the liquid-filled thin-walled steel cylindrical tanks decrease significantly when the *D/t* ratios increase. The *H/D* ratio also seems to have a negative effect on the seismic buckling strength; however, its effect is less significant than the D/t ratio.

CHAPTER 5 Seismic Analysis of Double-Skin Thin-Walled Composite Tanks (DSTWCTs)

5.1 Introduction

This chapter aims to study the seismic buckling behaviors of double-skin thin-walled composite tanks (DSTWCTs) with infill concrete between steel skins under horizontal earthquake excitations. Some researchers studied the concrete-filled double-skin steel tube as a column or beam-column. Seismic and static behaviors of the concrete-filled double skin steel tubes (CFDSTs) have been investigated in previous studies. The behaviors of concrete-filled steel columns under compression have been studied previously (Mamaghani, 2012; Mamaghani et al., 2009, 2014, 2016; Han et al., 2008; Yang and Han, 2009; Yang and Han, 2011). From previous studies, CFDSTs showed outstanding characteristics as structural bridge piers (Mamaghani, 2012; Mamaghani et al., 2009, 2014, 2016) and building columns (Cao and Wang, 2014; Yagishita et al., 2000; Zhang et al., 2015). Numerical models were developed to study the static and cyclic behavior of CFDST columns, and the sandwiched interaction between concrete and steel tubes was analyzed (Huang et al., 2010; Han et al., 2009). However, the knowledge of the seismic response of CFDST under real earthquake excitation is very limited. This study proposes the new design of the CFDST in terms of the double-skin thin-walled composite tanks (DSTWCTs) under earthquake excitations. The DSTWCT is designed to have the same diameter (D) and height (H) as a single-skin thin-walled steel tank (SSTWST) with an equal volume of steel. DSTWCT consists of two skins which are inner and outer walls. The inner diameter of DSTWCT is equal to the diameter of SSTWST. The steel volumes of the inner and outer walls of DSTWC are equal to 60% and 40% of the SSTWST, respectively. Fifteen different geometrical configurations of DSTWCT and three different geometrical configurations of the single-skin thin-walled steel tank (SSTWST)

were analyzed to investigate the seismic buckling behaviors of DSTWCTs. This chapter consists of three different DSTWCTs with height-to-diameter (*H/D*) ratios of 0.43, 0.67, and 1.00 and the diameter-to-thickness (*D/t*) ratios of 910, 1216, and 1521 to investigate the buckling behaviors of various sizes of DSTWCTs. The DSTWCTs were filled with concrete at 0%, 25%, 50%, 75%, and 100% of the heights of the DSTWCTs. The results show that the seismic buckling capacity of DSTWCT improves if the DSTWCT is filled with concrete by at least 50% of the height of the tank. The seismic buckling of DSTWCT takes place above the infill concrete level in the hollow section and moves to a higher location as the infill concrete level increases.

5.2 Methodology

5.2.1 Numerical Models of Double-Skin Thin-Walled Composite Tanks (DSTWCTs)

Fifteen different geometrical configurations of DSTWCT and three different geometrical configurations of SSTWST were analyzed to investigate the seismic buckling behaviors of DSTWCTs. The geometries of the cylindrical tanks are shown in Table 5.1 and illustrated in Fig. 5.1. This chapter consists of three different DSTWCTs with height-to-diameter (H/D) ratios of 0.43, 0.67, and 1.00 and the diameter-to-thickness (D/t) ratios of 910, 1216, and 1521 to investigate the buckling behaviors of various sizes of DSTWCTs. The DSTWCTs were filled with concrete at 0%, 25%, 50%, 75%, and 100% of the heights of the DSTWCTs. The thickness of the concrete-filled is considered as 5% of the inner diameter of DSTWCT. For the example of nomenclature, DSTWCT1-20 denotes DSTWCT1 with concrete-filled between inner and outer walls at 50% of the height of the tank.

The material for the walls and roofs of SSTWSTs and DSTWCTs is structural steel. The liquid inside the SSTWTs and DSTWCTs is water. The material properties of the structural steel

and water are identical to the material properties discussed in section 2.2.1. The concrete-filled between the inner and outer walls of DSTWCTs is the concrete with the mass density, ρ = 2,300 kg/m^3, compressive strength = 34.5 MPa, tensile strength = 4 MPa, modulus of elasticity, E = 28 GPa, and Poisson's ratio, ν = 0.20. All SSTWTs and DSTWCTs are filled with water up to 90% of the heights.

The commercial finite element program ANSYS was used to carry all computations. SHELL181 element was used for the walls and roofs of the SSTWSTs and DSTWCTs. SOLID185 element is used for the water-filled inside the cylindrical tanks. SOLID65 element was used for the concrete-filled between the inner and outer walls of DSTWCT. The numbers of elements for each CFDST with different ratios of concrete-filled are listed in Table 5.2. Figs. 5.2(a), 5.2(b), and 5.2(c) show the examples of meshing of the outer wall, inner wall, and concrete-filled of DSTWCT1-25, respectively.

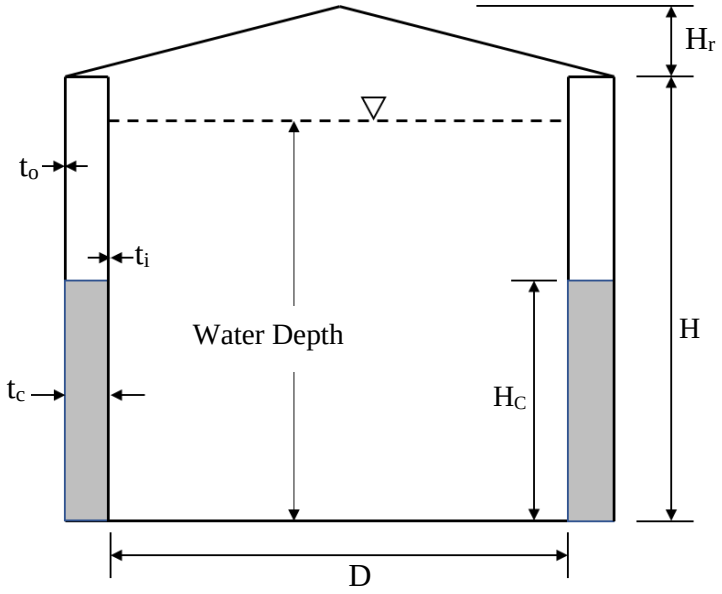

Fig. 5.1. Geometry of DSTWCT.

D

Table 5.1. Geometries of SSTWSTs and DSTWCTs

Tanks	***H*** **(m)**	***D*** **(m)**	***t*** **(mm)**	t_i **(mm)**	t_o **(mm)**	H_r **(m)**	***H/D***	***D/t***	H_c/H
SSTWST1	6.1	9.1	10.0	-	-	0.853	0.67	910	-
DSTWCT1-0	6.1	9.1	-	6.0	3.6	0.853	0.67	910	0.00
DSTWCT1-25	6.1	9.1	-	6.0	3.6	0.853	0.67	910	0.25
DSTWCT1-50	6.1	9.1	-	6.0	3.6	0.853	0.67	910	0.50
DSTWCT1-75	6.1	9.1	-	6.0	3.6	0.853	0.67	910	0.75
DSTWCT1-100	6.1	9.1	-	6.0	3.6	0.853	0.67	910	1.00
SSTWST2	15.2	15.2	12.5	-	-	1.425	1.00	1216	-
DSTWCT2-0	15.2	15.2	-	7.5	4.6	1.425	1.00	1216	0.00
DSTWCT2-25	15.2	15.2	-	7.5	4.6	1.425	1.00	1216	0.25
DSTWCT2-50	15.2	15.2	-	7.5	4.6	1.425	1.00	1216	0.50
DSTWCT2-75	15.2	15.2	-	7.5	4.6	1.425	1.00	1216	0.75
DSTWCT2-100	15.2	15.2	-	7.5	4.6	1.425	1.00	1216	1.00
SSTWST3	9.1	21.3	14.0	-	-	2.000	0.43	1521	-
DSTWCT3-0	9.1	21.3	-	8.4	5.0	2.000	0.43	1521	0.00
DSTWCT3-25	9.1	21.3	-	8.4	5.0	2.000	0.43	1521	0.25
DSTWCT3-50	9.1	21.3	-	8.4	5.0	2.000	0.43	1521	0.50
DSTWCT3-75	9.1	21.3	-	8.4	5.0	2.000	0.43	1521	0.75
DSTWCT3-100	9.1	21.3	-	8.4	5.0	2.000	0.43	1521	1.00

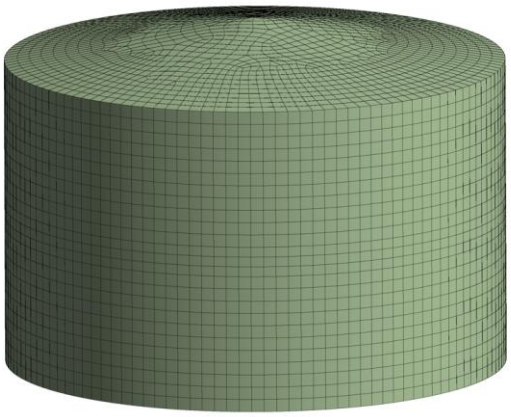

(a)

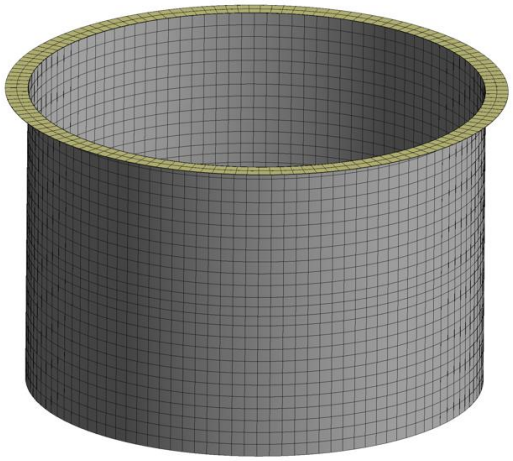

(b)

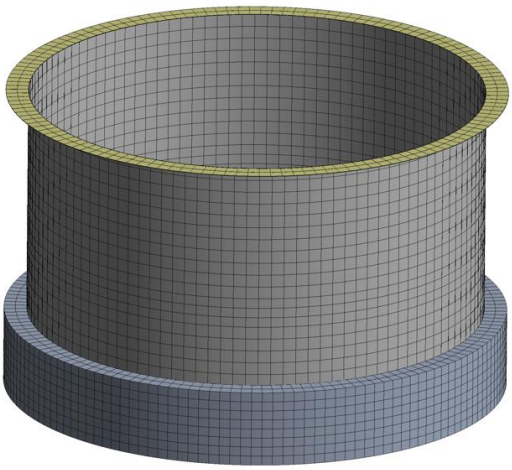

(c)

Fig. 5.2. DSTWCT1-25; (a) outer wall and roof, (b) inner wall, and (c) concrete-filled

Table 5.2. Elements of SSTWSTs and DSTWCTs

Tanks	SHELL181	SOLID65	SOLID185
SSTWST1	4174	0	1274
DSTWCT1-0	8605	0	1274
DSTWCT1-25	8605	2368	1274
DSTWCT1-50	8605	4736	1274
DSTWCT1-75	8605	7104	1274
DSTWCT1-100	8605	9472	1274
SSTWST2	8838	0	2076
DSTWCT2-0	18206	0	2076
DSTWCT2-25	18206	3072	2076
DSTWCT2-50	18206	6144	2076
DSTWCT2-75	18206	9216	2076
DSTWCT2-100	18206	12288	2076
SSTWST3	7198	0	1834
DSTWCT3-0	14972	0	1834
DSTWCT3-25	14972	2876	1834
DSTWCT3-50	14972	5752	1834
DSTWCT3-75	14972	8628	1834
DSTWCT3-100	14972	11504	1834

5.2.2 First Natural frequencies and Damping Ratios

Results from the modal analysis show that the natural frequency increases and the first mode shape also changes when the concrete-filled in DSTWCT increases. The increases of the first natural frequencies are represented in Table 5.3. Figs. 5.3(a), 5.3(b), and 5.3(c) illustrate the first mode shapes of DSTWCT2-0, DSTWCT2-50, and DSTWCT2-100, respectively. The natural frequencies and mode shapes are the parameters that are used to find mass coefficients for the

Rayleigh damping method in the transient analysis. In this study, the value of 2% was adopted. This mass coefficient (a_0) is put into the transient analysis to indicate the damping ratio of the structure. Table 5.3 shows the calculated mass coefficients (a_0) for the DSTWCTs with different concrete-filled ratios.

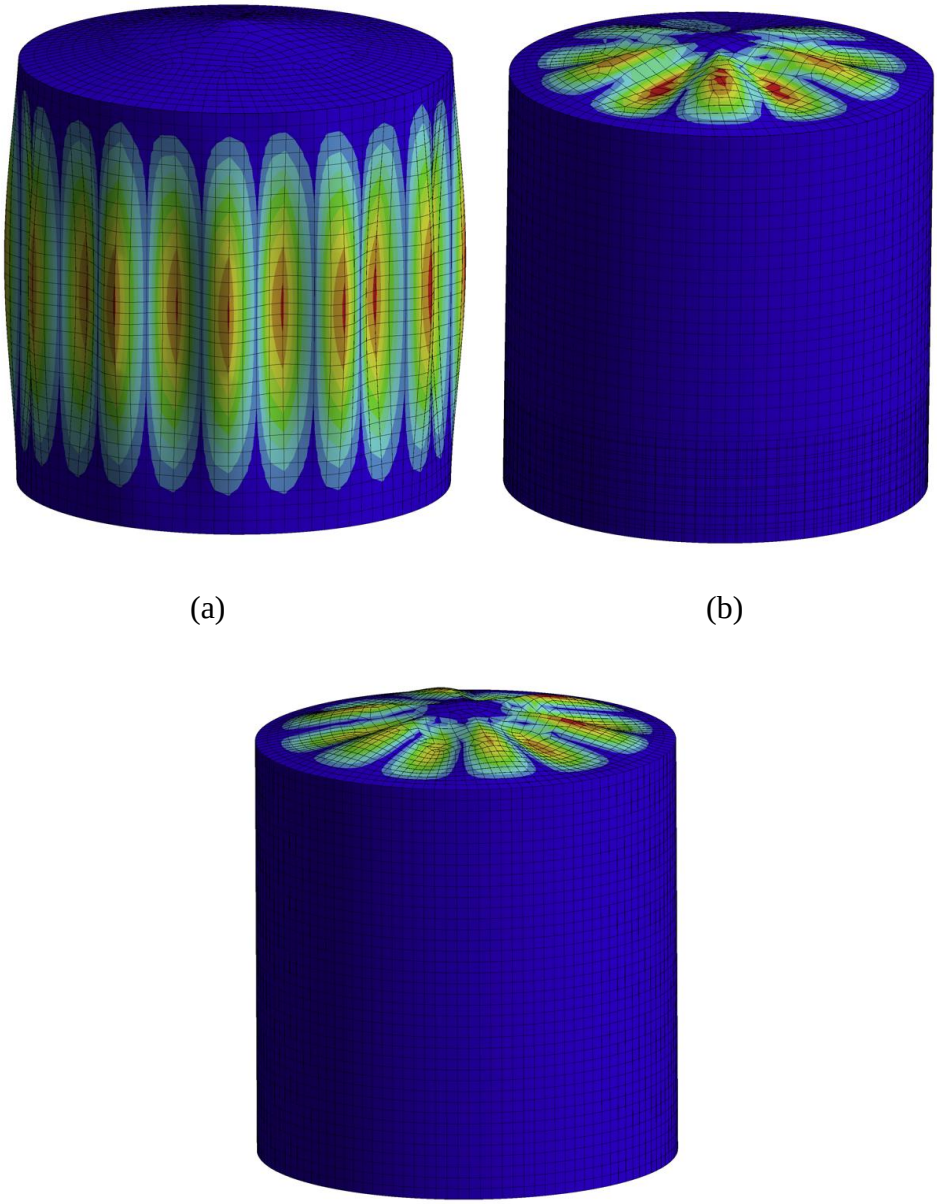

(a) (b)

(c)

Fig. 5.3. The first mode shapes of DSTWCT2; (a) DSTWCT2-0, (b) DSTWCT2-50, (c) DSTWCT2-100

Table 5.3 The first natural. frequencies and mass coefficients

Tanks	1st Natural frequencies (Hz)	a_0
SSTWST1	4.259	1.070
DSTWCT1-0	4.104	1.031
DSTWCT1-25	4.673	1.174
DSTWCT1-50	5.249	1.319
DSTWCT1-75	5.431	1.365
DSTWCT1-100	5.804	1.459
SSTWST2	2.293	0.576
DSTWCT2-0	2.784	0.700
DSTWCT2-25	3.259	0.819
DSTWCT2-50	4.648	1.168
DSTWCT2-75	5.836	1.467
DSTWCT2-100	6.781	1.704
SSTWST3	2.070	0.611
DSTWCT3-0	2.146	0.539
DSTWCT3-25	2.377	0.597
DSTWCT3-50	2.945	0.740
DSTWCT3-75	3.381	0.850
DSTWCT3-100	3.783	0.951

5.3 Seismic Buckling Results

The time-history in terms of the accelerogram of the El Centro Earthquake 1940 was used to be the applied load for both SSTWSTs and DSTWCTs. The accelerogram of the El Centro earthquake is illustrated in Fig 2.8.

5.3.1 SSTWST1 and DSTWCT1

A node that has the maximum displacement from each PGA is tracked. This displacement response was used to create the pseudo equilibrium path. The maximum displacement of DSTWCT1-25 can be observed as shown in Fig. 5.4, DSTWCT1-25 at node 2723 has maximum displacement when PGA is 0.8g. The results indicate that the seismic buckling occurs at the inner wall of DSTWCT1-25 as shown in Fig. 5.4. Fig. 5.5 shows the deformation shape of the outer wall and roof of DSTWCT1-25. It shows that the seismic buckling does not occur for the outer wall and roof of DSTWCT1-25 when it is subject to the El Centro earthquake accelerogram with PGA = 0.8g. Fig. 5.6 illustrates the pseudo-equilibrium paths and the seismic buckling capacities of SSTWST1 and DSTWCT1. Fig. 5.6 illustrates the pseudo-equilibrium path and the seismic buckling capacity of SSTWST1. The seismic buckling value of SSTWST1 is 0.72g. The numerical values in Fig. 5.6 can be obtained from the maximum displacement of the walls and roofs of SSTWST1 and DSTWCT1s.

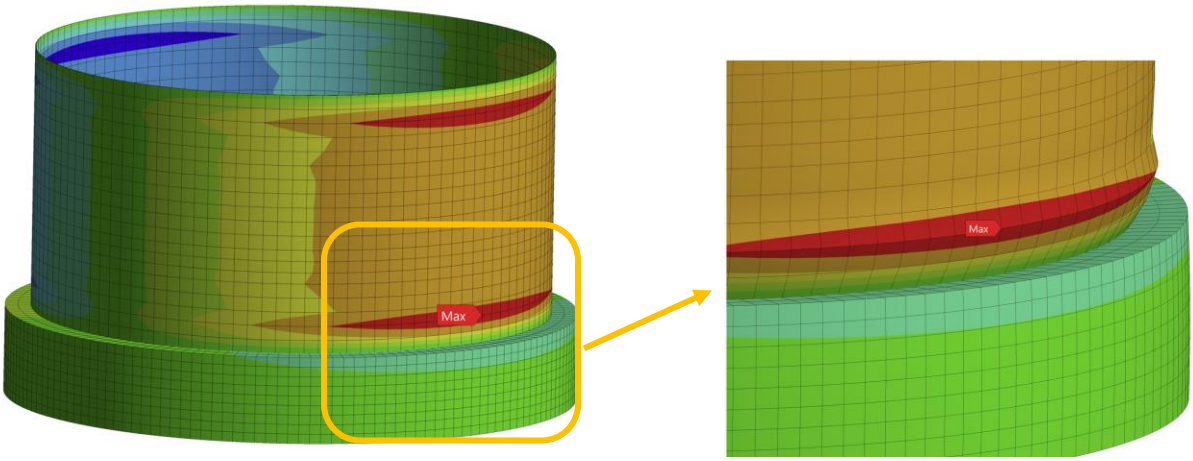

Fig. 5.4. Inner wall displacement of DSTWCT1-25 subjected to the El Centro earthquake at PGA = 0.8g.

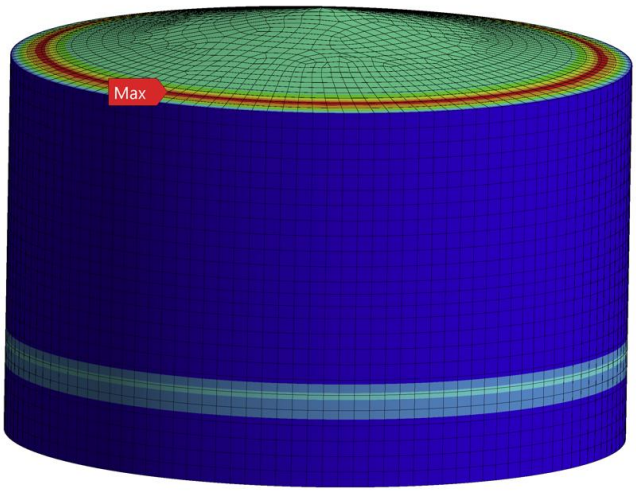

Fig. 5.5. Outer wall displacement of DSTWCT1-25 subjected to the El Centro earthquake at 0.8g.

Fig. 5.6(a) illustrates the pseudo-equilibrium paths and the seismic buckling capacities of SSTWST1 and DSTWCT1-0. The seismic buckling capacities of SSTWST1 and DSTWCT1-0 are 0.72g and 0.53g, respectively. Fig. 5.6(b) illustrates the pseudo-equilibrium paths and the seismic buckling capacities of DSTWCT1-25 and DSTWCT1-50. The seismic buckling capacities of DSTWCT1-25 and DSTWCT1-50 are 0.67g and 0.81G, respectively. Fig. 5.6(c) illustrates the pseudo-equilibrium paths and the seismic buckling capacities of DSTWCT1-75 and DSTWCT1-100. The seismic buckling capacities of DSTWCT1-75 and DSTWCT1-100 are 0.93g and 1.06g, respectively. The von-Mises stresses at the first instability points do not reach the yield stress for any tank since the yield stress in this study is assumed to be 345 MPa, which is equal to ASTM A572 steel (ASTM, 2018).

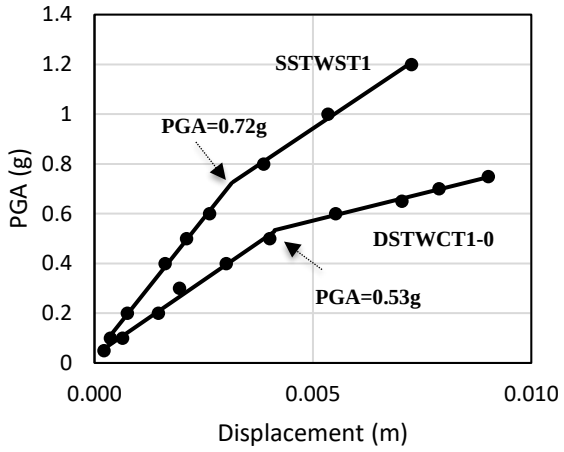

(a)

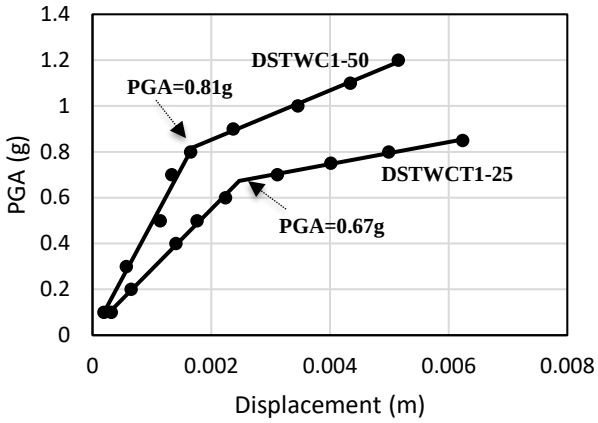

(b)

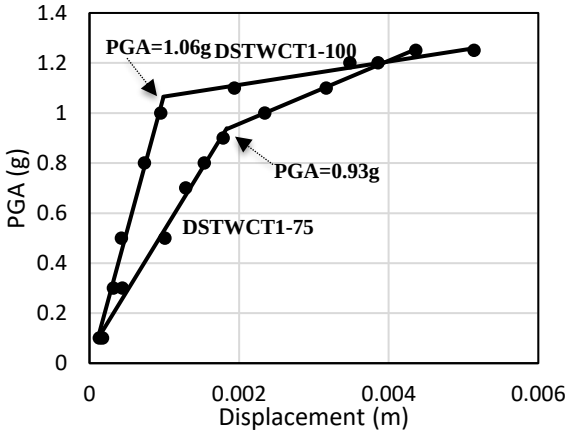

(c)

Fig. 5.6. Pseudo-equilibrium paths; (a) SSTWST1 and DSTWCT1-0, (b) DSTWCT1-25 and DSTWCT1-50, (c) DSTWCT1-75 and DSTWCT1-100.

5.3.2 SSTWST2 and DSTWCT2

Fig. 5.7 shows the example of the deformation shape of DSTWCT2-50 when it was subjected to the El Centro earthquake at PGA = 0.65g. The maximum displacement of DSTWCT2-50 can be observed as shown in Fig. 5.7(b), DSTWCT2-50 at node 9984 has maximum displacement when PGA is 0.65g. The results indicate that the seismic buckling occurs at the inner wall of DSTWCT2-50 as shown in Figs. 5.7(b) and 5.7(c). Fig. 5.7(a) shows the deformation shape of the outer wall and roof of DSTWCT2-50. It shows that the seismic buckling does not occur for the outer wall and roof of DSTWCT2-50 when it is subjected to the El Centro earthquake accelerogram with PGA = 0.65g. Fig. 5.8 illustrates the pseudo-equilibrium paths and the seismic buckling capacities of SSTWST2 and DSTWCT2. The seismic buckling capacity of SSTWST2 is 0.56g. The numerical values in Fig. 5.8 can be obtained from the maximum displacement of the walls and roofs of SSTWST2 and DSTWCT2s.

Fig. 5.8(a) illustrates the pseudo-equilibrium paths and the seismic buckling capacities of STTWST2 and DSTWCT2-0. The seismic buckling capacities of STTWST2 and DSTWCT2-0 are 0.56g, and 0.41g, respectively. Fig. 5.8(b) illustrates the pseudo-equilibrium paths and the seismic buckling capacities of DSTWCT2-25 and DSTWCT2-50. The seismic buckling capacities of DSTWCT2-25 and DSTWCT2-50 are 0.45g and 0.60g, respectively. Fig. 5.8(c) illustrates the pseudo-equilibrium paths and the seismic buckling capacities of DSTWCT2-75 and DSTWCT2-100. The seismic buckling capacities of DSTWCT2-75 and DSTWCT2-100 are 0.93g and 1.06g, respectively. The von-Mises stresses at the first instability points do not reach the yield stress for any tank.

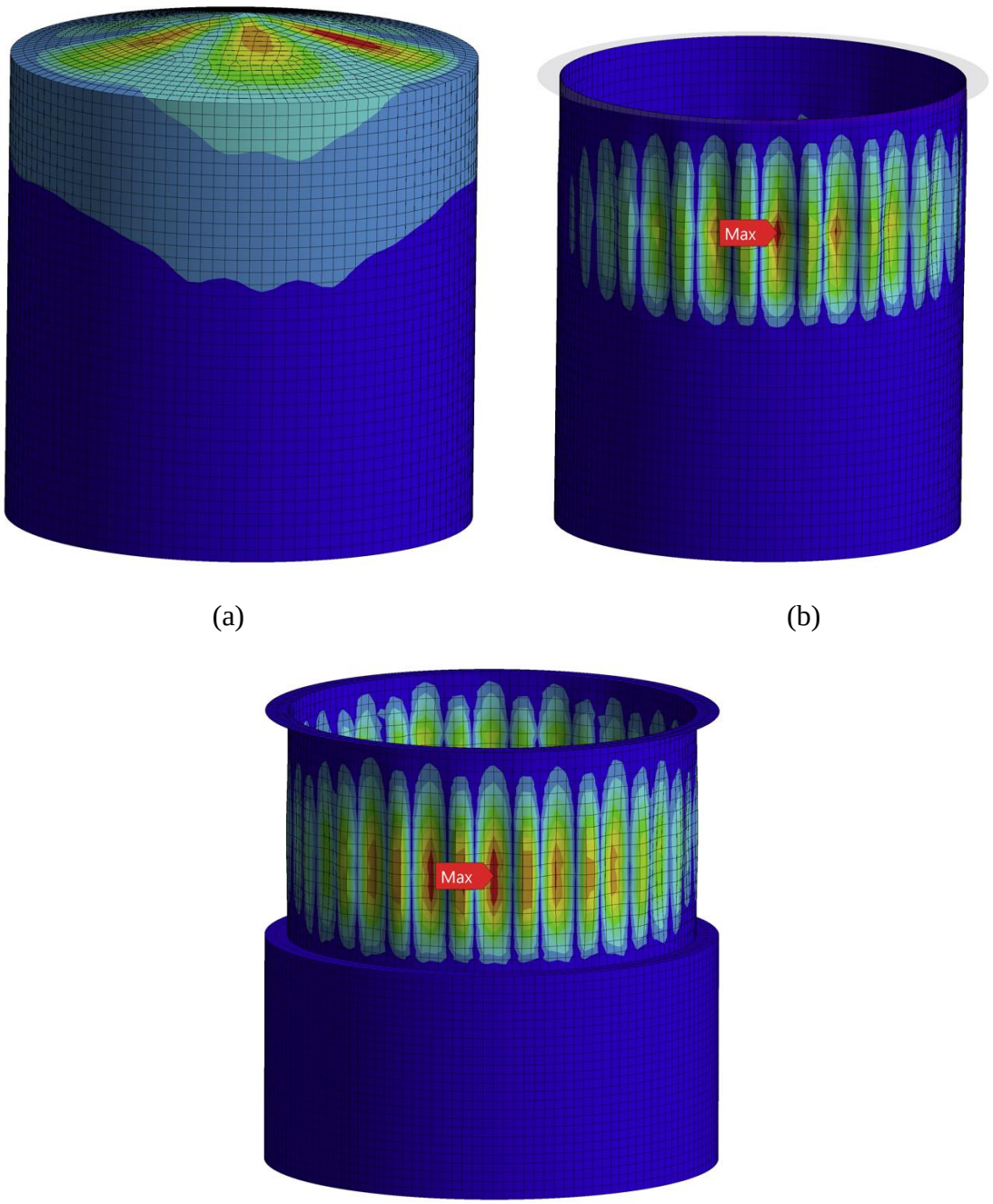

(a) (b)

(c)

Fig. 5.7. Displacement of DSTWCT2-50 subjected to the El Centro earthquake at PGA = 0.65g; (a) outer wall, (b) inner wall, and (c) inner wall and concrete-filled.

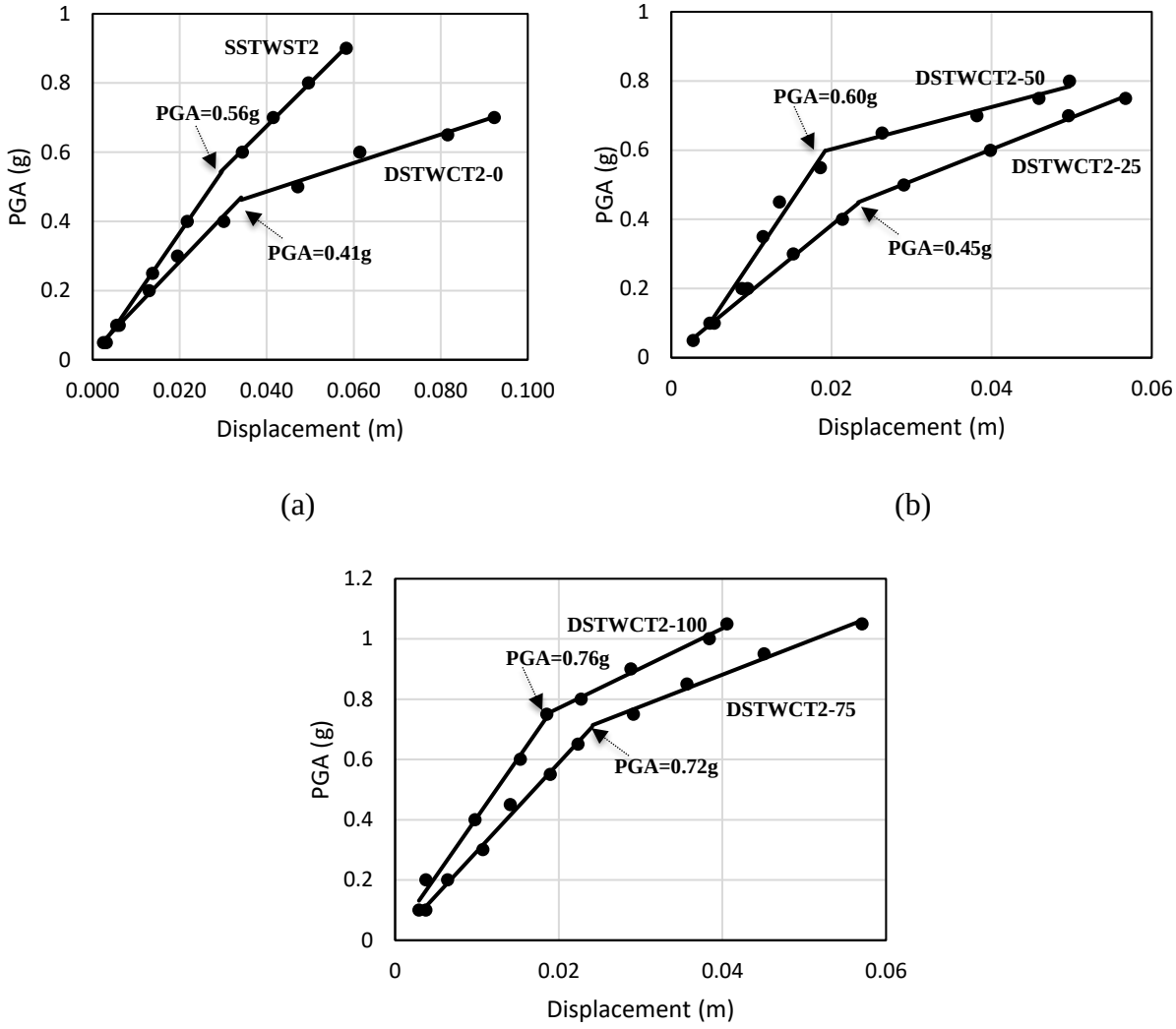

Fig. 5.8. Pseudo-equilibrium paths; (a) SSTWST2 and DSTWCT2-0, (b) DSTWCT2-25 and DSTWCT2-50, (c) DSTWCT2-75 and DSTWCT2-100.

5.3.3 SSTWST3 and DSTWCT3

Fig. 5.9(a) illustrates the pseudo-equilibrium paths and the seismic buckling capacities of STTWST3 and DSTWCT3-0. The seismic buckling capacities of STTWT3 and DSTWCT3-0 are 0.18g and 0.15g, respectively. Fig. 5.9(b) illustrates the pseudo-equilibrium paths and the seismic buckling capacities of DSTWCT3-25 and DSTWCT3-50. The seismic buckling capacities of DSTWCT3-25 and DSTWCT3-50 are 0.16g and 0.24g, respectively. Fig. 5.9(c) illustrates the pseudo-equilibrium paths and the seismic buckling capacities of DSTWCT3-75 and DSTWCT3-100. The seismic buckling capacities of DSTWCT3-75 and DSTWCT3-100 are 0.27g and 0.29g, respectively. The von-Mises stresses at the first instability points do not reach the yield stress.

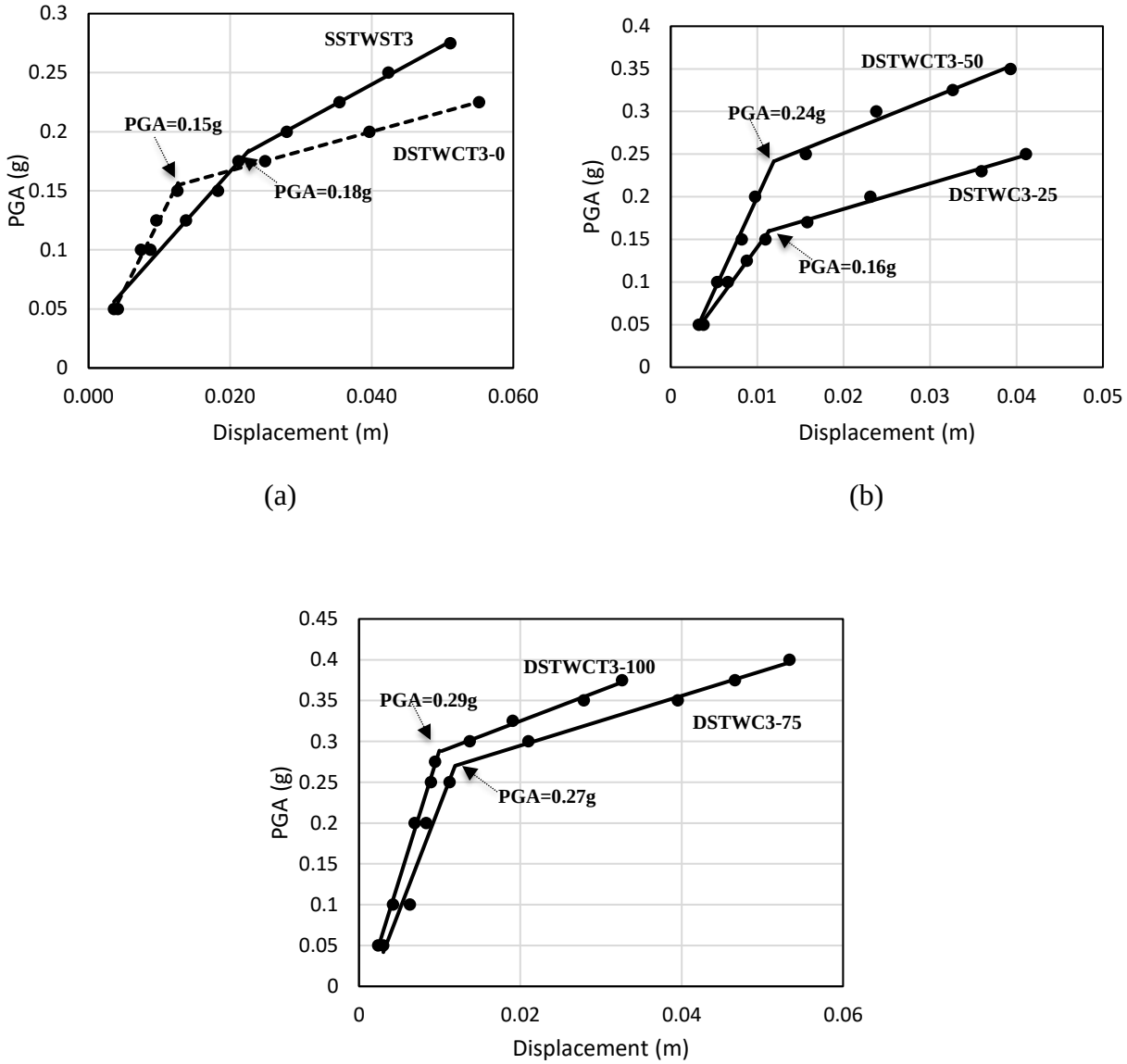

Fig. 5.9. Pseudo-equilibrium paths; (a) SSTWST3 and DSTWCT3-0, (b) DSTWCT3-25 and DSTWCT3-50, (c) DSTWCT3-75 and DSTWCT3-100.

5.4 Proposed Design Equation

To estimate the interaction effects of concrete-filled ratio on the seismic buckling strengths of the DSTWCTs, nonlinear regression analysis was used to develop a proposed design equation. The design equation can be estimated as Eq. (5.1).

$$PGA = -0.0692\ln(H/D) - 3.68(10^{-7})(D/t)^2 + 0.3295(H_c/H)^{1.875} + 1.006 \quad (5.1)$$

R^2 value of Eq. (5.1) is 0.940. The coefficients of *D/t* and H_c/H ratios are statistically significant at a 95% confident interval. However, the coefficient of H/D ratio is not statistically significant at 90% confident interval due to the change of slenderness ratio. From Eq. (5.1), H_c/H ratio has a significant positive effect which can improve the buckling capacity. For *D/t* and *H/D* ratios, if the D/t ratio increases, the dynamic buckling capacity significantly decreases. An increase in the H/D ratio also shows a negative effect on dynamic buckling capacity; however, when the H/D ratio increases the buckling capacity decreases with a diminishing rate.

5.5 Summary

This study showed that the effects of the H_c/H ratio on the seismic buckling capacities of the DSTWCTs, and the H_c/H ratio can improve the seismic buckling strength of the liquid-filled thin-walled steel tanks. Some of the main points are:

1. The seismic buckling capacity of DSTWCT improves if the DSTWCT is filled with concrete at least 50% of the height of the tank. The seismic buckling of DSTWCT takes place above the infill concrete level in the hollow section and moves to a higher location as the infill concrete level increases.

2. The results indicate that DSTWCT with H_c/H less than 0.5 has less seismic buckling capacity compared to the conventional liquid-filled thin-walled steel tanks as presented in chapters 2 and 3.
3. When the gap between the inner and outer walls of the DSTWCT is filled with concrete less than 50% of the height, the seismic buckling occurs at the inner wall of the DSTWCT. On the other hand, when the gap between the inner and outer walls of the DSTWCT is filled with concrete more than 50% of the height, the seismic buckling occurs at the roof of the DSTWCT. The von-Mises stresses at the first instability points do not reach the yield stress.

CHAPTER 6 Conclusions, Recommendations, and Future Work

The seismic behaviors of the liquid-filled thin-walled steel cylindrical tanks were investigated. The extensive parameters related to the seismic buckling behavior of the liquid-filled thin-walled steel cylindrical tanks were analyzed. Based on the compressive work of this dissertation, the knowledge of the seismic response of the liquid-filled thin-walled steel cylindrical tanks in terms of *D/t* ratio, *H/D* ratio, and geometric imperfection has been expanded and fulfilled. Moreover, the new design methods to improve the seismic strength of the liquid-filled thin-walled steel cylindrical tanks were proposed, which are the designs of stiffened liquid-filled thin-walled steel cylindrical tank and double-skin thin-walled composite tank (DSTWCT). The following conclusions are drawn:

- The accuracy of FEM was ensured with the existing experimental and theoretical equation. The result for FEA shows a good agreement with both the experimental result and theoretical equation.
- The interaction effects of *D/t* and *H/D* ratios on the seismic buckling were investigated, and estimated design equations were proposed. Results showed that the *D/t* ratio is an important parametric factor of the seismic buckling strength of the liquid-filled thin-walled steel cylindrical tank. The seismic buckling capacity of the tank decreases significantly when the *D/t* ratio increases. An increase in the H/D ratio also seems to have a negative effect on the seismic buckling strength; however, its effect is less significant compared to the *D/t* ratio.
- The initial geometric imperfection significantly reduces the seismic buckling capacity of the tank in the range between 5% to 33%.

- The vertical stiffeners improve the seismic buckling strength of the liquid-filled thin-walled steel cylindrical tanks when they are subjected to horizontal earthquake excitation. The vertical stiffeners can improve the seismic buckling strength by at least 10% of the critical PGA of unstiffened liquid-filled thin-walled steel cylindrical tanks. The von-Mises stresses at the first instability points do not reach the yield stress.
- The seismic buckling capacity of the DSTWCTs develops if the DSTWCT is filled with concrete by 50% of the height of the tank. The location of the seismic buckling of each analyzed DSTWCT moves to the higher location related to the H_c/H ratio. The results indicate that CFDST with H_c/H less than 0.5 has less seismic buckling capacity compared to the conventional liquid-filled thin-walled steel tanks.
- When the gap between the inner and outer walls of the DSTWCT is filled with concrete less than 50% of the height, the seismic buckling occurs at the inner wall of the DSTWCT. On the other hand, when the gap between the inner and outer walls of the DSTWCT is filled with concrete more than 50% of the height, the seismic buckling occurs at the roof of the DSTWCT.

6.1 Recommendations

- Design equations may have to be reinvestigated if the dimension of the liquid-fill thin-walled steel cylindrical tank is not covered by this study.
- To expand the knowledge of the seismic behavior of the stiffened liquid-filled thin-walled steel cylindrical tanks, the number of vertical stiffeners can be adjusted, and the stiffener rings can be included.

- The thickness of the concrete-filled between the inner and outer walls of DSTWCTs may be adjusted to investigate the seismic behavior of DSTWCTs based on the different thickness ratios of concrete-filled.

6.2 Future work

The future step of this study is to set up the experimentation on the liquid-filled thin-walled steel cylindrical tank to validate the numerical analysis and introduce the practical design code. Additionally, the extensive study of the effects of thickness ratios of concrete-filled in between inner and outer walls the steel wall thickness of DSTWCT will be investigated.

REFERENCES

American Lifelines Alliance (2001). Seismic fragility formulations for water systems. ASCE. Part1-Guideline, Part-2 Appendices.

ANSYS, Inc. (2009). ANSYS training manual.

ASTM A572 / A572M-18. (2018). Standard Specification for High-Strength Low-Alloy Columbium-Vanadium Structural Steel, ASTM International, West Conshohocken, PA, 2018, www.astm.org

Auli W, Rammerstorfer FG. (1986). On the dynamic instability of shell structures - criteria and algorithms. In: Finite element methods for plate and shell structures. Formulations and algorithms, vol. 2. Swansea (UK): Pineridge Press; p. 48–52.

British Standards Institution. (2005). *Eurocode 3: Design of steel structures*. London: BSI.

Budiansky, B., Roth, RS., (1962). Axisymmetric dynamic buckling of clamped shallow spherical shells. *NASA TN*, *1510*, 597-606.

Buratti, N., Tavano, M. (2014). Dynamic buckling and seismic fragility of anchored steel tanks by the added mass method. *Earthquake Engineering & Structural Dynamics*, *43*(1), 1-21.

Burgos, C. A., Batista-Abreu, J. C., Calabr_o, H. D., Jaca, R. C., and Godoy, L.A. (2015)., Buckling Estimates for Oil Storage Tanks: Effect of Simplified Modeling of the Roof and Wind Girder, *Thin-Walled Struct.*, 91, pp. 29–37.

Cao, H. Y., Wang, R. (2014). Finite element analysis of concrete filled double-skin (CHS inner and CHS outer) steel tubes under lateral impact. In *Applied Mechanics and Materials* (Vol. 501, pp. 704-709). Trans Tech Publications Ltd.

Chopra, A. K. (2011). Dynamics of structures: theory and application to earthquake engineering. 4th ed., Prentice Hall.

Cooper TW, Wachholz TP. (1999). Optimizing post-earthquake lifeline system reliability. *In Proceedings of the 5th US conference on lifeline earthquake engineering*. ASCE, vol. 16. p. 878–86.

Djermane, M., D. Zaoui, B. Labbaci, and F. Hammadi. (2014). Dynamic buckling of steel tanks under seismic excitation: Numerical evaluation of code provisions. *Engineering Structures,* 70: 181-196.

Donnell LH, Wan CC. Effect of imperfection on buckling of thin cylinders and columns under axial compression. J Appl Mech 1950;17:73–83.

Fischer, E. C., Liu, J., & Varma, A. H. (2016). Investigation of cylindrical steel tank damage at wineries during earthquakes: Lessons learned and mitigation opportunities. *Practice Periodical on Structural Design and Construction*, *21*(3).

Han, L. H., Huang, H., & Zhao, X. L. (2009). Analytical behaviour of concrete-filled double skin steel tubular (CFDST) beam-columns under cyclic loading. *Thin-walled structures*, *47*(67), 668-680.

Han, L. H., Liu, W., Yang, Y. F. (2008). Behaviour of concrete-filled steel tubular stub columns subjected to axially local compression. *Journal of Constructional Steel Research*, *64*(4), 377-387.

Handam F. H. (2000). Seismic behavior of cylindrical steel storage tanks. *Journal of Construction Steel Research*, 53: 307–33.

Housner GW, Haroun MA. (1979). Vibration tests of full-scale liquid storage tanks, *Proceedings of the second United States national conference on earthquake engineering*.

Housner GW. (1963). The Dynamic Behavior of Water Tanks. Bulletin of the Seismological Society of America; 53(2):381–9.

Huang, H., Han, L. H., Tao, Z., & Zhao, X. L. (2010). Analytical behaviour of concrete-filled double skin steel tubular (CFDST) stub columns. *Journal of Constructional Steel Research*, *66*(4), 542-555.

Index to NSMP Data Sets. (2014, March 19). Retrieved April 25, 2017, from https://escweb.wr.usgs.NSgov/nsmp-data/

Jerath, S., Lee, M. (2015). Stability analysis of cylindrical tanks under static and earthquake loading. *Journal of Civil Engineering and Architecture*, *9*(1), 72-79.

Johnson, H. (2019). Earthquake Loading Effects on The Buckling of Liquid Filled Cylindrical Storage Tanks. *The University of North Dakota*.

Kebeli, H. V., (2002). Determining Pressure Coefficients Due to Wind Loading On Grain Bins. Ph.D. thesis, *University of Florida, Gainesville, FL*.

Kim, S. E., Kim, C. S. (2002). Buckling strength of the cylindrical shell and tank subjected to axially compressive loads. *Thin-walled structures*, *40*(4), 329-353.

Malhotra P, Veletsos AS. (1994). Uplifting response of unanchored liquid storage tanks. ASCE *Journal of Structural Engineering*, 120(12):3525–47.

Mamaghani, I. H.P., & Abdulrazzak, A. (2014). Seismic Design of Partially Concrete-Filled Steel Box Bridge Piers. *Journal of Transportation Research Board*, No. 14-3804, p1-9.

Mamaghani, I.H.P**.** (2012). Innovative Performance-Based Seismic Design Methodologies for American Bridge Piers using Partially Concrete-Filled Steel Tubular Columns. *ASCE Committee on Steel Bridges*, Chicago, *Invited Paper*, March 30, 2012

Mamaghani, I.H.P., Erdogan, E., Nemati, N., and Shokri, T. (2009). Inelastic Analysis and Ductility Evaluation of Partially Concrete-Filled Steel Tubular Columns under Cyclic Loading, *Structural Stability Research Council*, April1-5, Phoenix, Arizona, pp. 471-490.

Mamaghani, I.H.P**.**, Wesley, K, Ahmad, F., Dorose, B. (2016). Local Buckling Restraining Behavior of Partially Concrete-filled Steel Tubular (CFST) Bridge Piers under Seismic Loads, *Istanbul Bridge Conference*, Istanbul, Turkey, August 8-10, Paper ID: 108.

Mandara A, Mazzolani M. Stocky cylinders if compression: postcritical path evaluation and collapse load prediction with ABAQUS. In: Proceedings of ABAQUS User's Conference, Archen, Germany 1993; 421–35.

Miller CD. Buckling of axially compressed cylinder. Proc ASCE, J Struct Div 1976;103(ST3):695–721.

Morita H, Ito T, Hamada K, Sugiyama A, Kawamoto Y, Ogo H et al. (2003). Investigation on buckling behavior of liquid storage tanks under seismic excitation: 2nd report Investigation on the nonlinear ovaling vibration at the upper wall. *Proceedings of the ASME pressure vessels and piping conference*, vol. 466. p. 227–34.

Natsiavas S, Babcock CD. (1987). Buckling at the top of a fluid-filled tank during base excitation. *ASME Journal of Pressure Vessel Technology*, 109: 374–80.

Niwa, Akira, and Ray W. Clough. (1982). Buckling of cylindrical liquid-storage tanks under earthquake loading. *Earthquake Engineering & Structural Dynamics* 10.1: 107-122.

Portela, G., and Godoy, L. A., 2005, "Wind Pressures and Buckling of Cylindrical Steel Tanks with a Conical Roof," J. Constr. Steel Res., 61(6), pp. 786–807.

Priestley, M. J. N., Davidson, B. J., Honey, G. D., Hopkins, D. C., Martin, R. J., Ramsey, G., & Wood, J. H. (1986). "Seismic design of storage tanks". Recommendations of a study group of the New Zealand National Society for Earthquake Engineering, 3.

Resinger, F., and Greiner, R., (1982). Buckling of Wind Loaded Cylindrical Shells—Application to Unstiffened and Ring-Stiffened Tanks, Buckling of Shells, Springer, Berlin, pp. 305–331.

Roopkumdee W, Mamaghani I. (2019). Seismic design and buckling strength evaluation of liquid-filled steel cylindrical tanks, *International Journal of Modern Engineering*, 19(1).

Roopkumdee W, Mamaghani I.H.P., and Jerath S. (2018). Buckling strength of liquid-filled steel cylindrical tanks under seismic load, *Proceedings of the 11th National Conference in Earthquake Engineering, Earthquake Engineering Research Institute*, Los Angeles, CA.

Roopkumdee, W. (2017). Buckling of liquid-filled steel storage tanks under earthquake loading. *The University of North Dakota*.

Roopkumdee, W., Mamaghani, I. H. P. (2021). Seismic Analysis of Double-Skin Thin-Walled Composite Tank (DSTWCT). *Engineering Structures*, (to be submitted).

Roopkumdee, W., Mamaghani H.P. I., (2021). Seismic Analysis of Perfect and Imperfect Cylindrical Liquid Storage Tanks. *International Journal of Civil Infrastructure*, 4, 173-179.

Sabransky, I. J., and Melbourne, W. H., 1987, Design Pressure Distribution on Circular Silos with Conical Roofs, J. Wind Eng. Ind. Aerodyn., 26(1), pp. 65–84.

Sezen, Halil, Ramazan Livaoglu, and Adem Dogangun. (2008). Dynamic analysis and seismic performance evaluation of above-ground liquid-containing tanks. *Engineering Structures* 30.3: 794-803. 2008.

Singer J. (1999). On the importance of shell buckling experiments. *J Appl Mech Rev* 1999;52(6):17–25.

Singiresu, S. R. (1995). *Mechanical vibrations*. Addison Wesley.

Sobhan, M. S., Fayaz R. Rofooei, and Nader KA Attari. (2017). Buckling behavior of the anchored steel tanks under horizontal and vertical ground motions using static pushover and incremental dynamic analyses. *Thin-Walled Structures* 112: 173-183.

Sun, T., Azzuni, E., & Guzey, S. (2018). Stability of open-topped storage tanks with top stiffener and one intermediate stiffener subject to wind loading. *Journal of Pressure Vessel Technology*, *140*(1).

Tazuke, H., Yamaguchi, S., Ishida, K., Sakurai, T., Akiyama, H. and Chiba, T., (2002). "Seismic proving test of equipment and structures in thermal conventional power plant*". J. Pressure Vessel Technol*., 124(2), pp.133-143.

Teng J. G., Rotter J. M. (2004). Buckling of thin metal shells. *London: Spon Press, Taylor and Francis*; 2004

Timoshenko SP, Gere JM. Theory of elastic stability. New York: McGraw-Hill, 1983.

Timoshenko SP, Woinowsky-Krieger S. Theory of plate and shell. New York: McGraw-Hill, 1959.

Uematsu, Y., Koo, C., and Yasunaga, J. (2014). Design Wind Force Coefficients for Open-Topped Oil Storage Tanks Focusing on the Wind-Induced Buckling, J. Wind Eng. Ind. Aerodyn., 130, pp. 16–29.

Virella JC, Su´arez LE, Godoy LA. (2005). Effect of pre-stress states on the impulsive modes of vibration of cylindrical tank–liquid systems under horizontal motions. *Journal of Vibration and Control*, 11(9).

Virella, J. C., L. A. Godoy, and L. E. Suárez. (2006). Dynamic buckling of anchored steel tanks subjected to horizontal earthquake excitation. *Journal of Constructional Steel Research*, 62.6: 521-531. 2006.

Yagishita, F., Kitoh, H., Sugimoto, M., Tanihira, T., and Sonoda, K. (2000). Double skin composite tubular columns subjected to cyclic horizontal force and constant axial force. In *Proc., 6th ASCCS Int. Conf. on Steel-Concrete Composite Structures* (pp. 497-503). Los Angeles: Univ. of Southern California.

Yang, Y. F., Han, L. H. (2009). Experiments on rectangular concrete-filled steel tubes loaded axially on a partially stressed cross-sectional area. *Journal of Constructional Steel Research*, *65*(8-9), 1617-1630.

Yang, Y. F., Han, L. H. (2011). Behaviour of concrete filled steel tubular (CFST) stub columns under eccentric partial compression. *Thin-Walled Structures*, *49*(2), 379-395.

Yang, Y. F., Han, L. H. (2012). Concrete filled steel tube (CFST) columns subjected to concentrically partial compression. *Thin-Walled Structures*, *50*(1), 147-156.

Yasunaga, J., Koo, C., and Uematsu, Y., 2012, "Wind Loads for Designing Cylindrical Storage Tanks—Part 1: Characteristics of Wind Pressure and Force Distributions," J. Wind Eng., 37(2), pp. 43–53.

Yasunaga, J., Koo, C., and Uematsu, Y., 2012, Wind Loads for Designing Cylindrical Storage Tanks—Part 2: Wind Force Model with Consideration of the Buckling Behavior Under Wind Loading, J. Wind Eng., 37(3), pp. 79–92.

Zhang, F., Wu, C., Zhao, X. L., Li, Z. X., Heidarpour, A., & Wang, H. (2015). Numerical modeling of concrete-filled double-skin steel square tubular columns under blast loading. *Journal of Performance of Constructed Facilities*, *29*(5), B4015002.

Zhao, Y., Lin, Y. (2014). “Buckling of Cylindrical Open-Topped Steel Tanks Under Wind Load,” Thin-Walled Structure., 79, pp. 83–94.